

1 **A SARS-CoV-2 spike ferritin nanoparticle vaccine protects against heterologous**
2 **challenge with B.1.1.7 and B.1.351 virus variants in Syrian golden hamsters**

3

4 Kathryn McGuckin Wuertz¹, Erica K. Barkei², Wei-Hung Chen^{3,4}, Elizabeth J. Martinez^{3,4}, Ines
5 Lakhal-Naouar^{4,5}, Linda L. Jagodzinski⁵, Dominic Paquin-Proulx^{1,4}, Gregory D. Gromowski⁶,
6 Isabella Swafford^{1,4}, Akshaya Ganesh^{1,7}, Ming Dong^{1,4}, Xiankun Zeng⁸, Paul V. Thomas^{3,4},
7 Rajeshwer S. Sankhala^{3,4}, Agnes Hajduczki^{3,4}, Caroline E. Peterson^{3,4}, Caitlin Kuklis⁶, Sandrine
8 Soman⁶, Lindsay Wieczorek^{1,4}, Michelle Zemil^{1,4}, Alexander Anderson^{3,7}, Janice Darden^{4,5},
9 Heather Hernandez^{4,5}, Hannah Grove^{4,5}, Vincent Dussupt^{1,4}, Holly Hack^{4,5}, Rafael de la Barrera⁹,
10 Stasya Zarling⁹, James F. Wood⁹, Jeffrey W. Froude⁹, Matthew Gagne¹⁰, Amy R. Henry¹⁰, Elham
11 Bayat Mokhtari¹¹, Prakriti Mudvari¹¹, Shelly J. Krebs^{1,4}, Andrew S. Pekosz¹², Jeffrey R. Currier⁶,
12 Swagata Kar¹³, Maciel Porto¹³, Adrienne Winn¹³, Kamil Radzyminski¹³, Mark G. Lewis¹³, Sandhya
13 Vasan⁴, Mehul Suthar¹⁴, Victoria R. Polonis¹, Gary R. Matyas¹, Eli A. Boritz¹¹, Daniel C. Douek¹⁰,
14 Robert A. Seder¹⁵, Sharon P. Daye¹⁶, Mangala Rao¹, Sheila A. Peel⁵, M. Gordon Joyce^{3,4,18}, Diane
15 L. Bolton^{1,4,18}, Nelson L. Michael^{17,18,*} and Kayvon Modjarrad^{3,18,*}

16

17 ¹U.S. Military HIV Research Program, Center for Infectious Diseases Research, Walter Reed Army Institute of
18 Research, Silver Spring, Maryland USA

19 ²Veterinary Pathology Division, Walter Reed Army Institute of Research, Silver Spring, Maryland USA

20 ³Emerging Infectious Diseases Branch, Center for Infectious Diseases Research, Walter Reed Army Institute of
21 Research, Silver Spring, Maryland USA

22 ⁴Henry M. Jackson Foundation for the Advancement of Military Medicine, Bethesda, Maryland USA

23 ⁵Diagnostics Countermeasures Branch, Center for Infectious Diseases Research, Walter Reed Army Institute of
24 Research, Silver Spring, Maryland USA

25 ⁶Virus Diseases Branch, Center for Infectious Diseases Research, Walter Reed Army Institute of Research, Silver
26 Spring, Maryland USA

27 ⁷Oak Ridge Institute of Science and Education, Oak Ridge, Tennessee USA

28 ⁸Pathology Division, United States Army Medical Research Institute of Infectious Diseases, Fort Detrick, Frederick,
29 Maryland USA

30 ⁹Pilot Bioproduction Facility, Walter Reed Army Institute of Research, Silver Spring, Maryland USA

31 ¹⁰Human Immunology Section, Vaccine Research Center, National Institute of Allergy and Infectious Diseases,
32 National Institutes of Health, Bethesda, Maryland USA

33 ¹¹Virus Persistence and Dynamics Section, Vaccine Research Center, National Institute of Allergy and Infectious
34 Diseases, National Institutes of Health, Bethesda, Maryland USA

35 ¹²W. Harry Feinstone Department of Molecular Microbiology and Immunology, Johns Hopkins Bloomberg School of
36 Public Health, Baltimore, Maryland USA

37 ¹³BioQual, Inc., Rockville, Maryland USA

38 ¹⁴Emory Vaccine Center, Department of Pediatrics, Emory School of Medicine, Atlanta, Georgia USA

39 ¹⁵Cellular Immunology Section, Vaccine Research Center, National Institute of Allergy and Infectious Diseases,
40 National Institutes of Health, Bethesda, Maryland USA

41 ¹⁶One Health Branch, Walter Reed Army Institute of Research, Silver Spring, Maryland USA

42 ¹⁷Center for Infectious Diseases Research, Walter Reed Army Institute of Research, Silver Spring, Maryland USA

43 ¹⁸These authors contributed equally.

44

45 *Corresponding authors:

46 Nelson L. Michael, M.D., Ph.D., nelson.l.michael2.civ@mail.mil

47 Kayvon Modjarrad, M.D., Ph.D., kayvon.modjarrad.civ@mail.mil

48 **Abstract**

49 **The emergence of SARS-CoV-2 variants of concern (VOC) requires adequate coverage of vaccine**
50 **protection. We evaluated whether a spike ferritin nanoparticle vaccine (SpFN), adjuvanted**
51 **with the Army Liposomal Formulation QS21 (ALFQ), conferred protection against the B.1.1.7**
52 **and B.1.351 VOCs in Syrian golden hamsters. SpFN-ALFQ was administered as either single or**
53 **double-vaccination (0 and 4 week) regimens, using a high (10 µg) or low (0.2 µg) immunogen**
54 **dose. Animals were intranasally challenged at week 11. Binding antibody responses were**
55 **comparable between high- and low-dose groups. Neutralizing antibody titers were equivalent**
56 **against WA1, B.1.1.7, and B.1.351 variants following two high dose two vaccinations. SpFN-**
57 **ALFQ vaccination protected against SARS-CoV-2-induced disease and viral replication following**
58 **intranasal B.1.1.7 or B.1.351 challenge, as evidenced by reduced weight loss, lung pathology,**
59 **and lung and nasal turbinate viral burden. These data support the development of SpFN-ALFQ**
60 **as a broadly protective, next-generation SARS-CoV-2 vaccine.**

61

62 **Introduction**

63 Since the beginning of the COVID-19 pandemic, an unprecedented global effort has resulted in
64 the rapid emergence, and early regulatory authorization or approval, of multiple vaccines for use
65 in humans¹. The emergence of variants of concern (VOC) underscores the need for continued
66 development of next-generation vaccines^{2,3}. Increasingly, VOCs are becoming the dominant
67 circulating lineages world-wide, owing to their increased transmissibility and potential to cause
68 breakthrough infection in vaccinated individuals. Two VOCs have gained particular attention:
69 B.1.1.7 and B.1.351, first detected in the United Kingdom and in the Republic of South Africa,
70 respectively⁴⁻¹⁰. Recent studies have shown markedly reduced cross-neutralizing antibody
71 responses from convalescent and vaccinee sera against both VOCs, but B.1.351 in particular
72 ^{4,5,8,11-14}. Consequently, there has been a renewed, global effort to new iterations of SARS-CoV-2
73 vaccines confer protection against current and emerging SARS-CoV-2 VOCs^{4,15,16}.

74
75 We recently developed a novel SARS-CoV-2 vaccine that presents eight prefusion-stabilized spike
76 glycoprotein trimers in an ordered array on a ferritin nanoparticle (SpFN) and adjuvanted with
77 Army Liposomal Formulation QS21 (ALFQ). This formulation has demonstrated efficacy against
78 the origin strain of SARS-CoV-2 (WA1) in both K18 murine and rhesus macaque viral challenge
79 models¹⁷⁻²⁰. In rhesus macaques, SpFN elicited a dose-dependent potent humoral and cellular
80 immune response that translated into a precipitous reduction in viral load upper and lower
81 airways of the animals, as well as protection from lung histopathology. Importantly,
82 immunization induced cross-neutralizing antibodies against current circulating VOCs¹⁸. Building
83 on these data, we evaluated the efficacy of SpFN-ALFQ to protect against virus challenge with

84 VOCs B.1.1.7 and B.1.351 in a Syrian golden hamster (SGH) challenge model . This animal model
85 has become a standard in the field for pre-clinical SARS-CoV-2 vaccine development, as
86 respiratory pathology in this model closely recapitulates human disease²¹⁻²⁴.

87

88 Here, we demonstrate that SpFN adjuvanted with ALFQ (SpFN-ALFQ) generates strong binding
89 antibody responses against the receptor binding domain and spike proteins of both B.1.1.7 and
90 B.1.351, as well as potent neutralizing antibody responses against both VOCs. Consistent with
91 development of a protective humoral response, we demonstrate that SpFN-ALFQ confers clear
92 protection against upper respiratory tract disease following challenge with these VOCs, as
93 demonstrated by less body weight loss and decreased tissue viral burden and lung pathology.
94 The SpFN vaccine candidate is now currently under assessment in a human phase 1 clinical trial
95 (ClinicalTrials.gov Identifier: NCT04784767). These data support further development of the
96 vaccine as one that may be broadly applicable to multiple sarbecovirus lineages.

97

98 **Results**

99

100 **Hamster model to assess efficacy of SpFN-ALFQ against B.1.1.7 and B.1.351**

101 Prior studies have demonstrated that the SpFN-ALFQ vaccine is efficacious against the WA1 strain
102 of SARS-CoV-2 in a nonhuman primate model¹⁸. The ability of this vaccine to confer protection
103 against the VOC B.1.1.7, now prominent throughout the U.S. and other parts of the world, and
104 B.1.351, prominent in Africa and emerging world-wide, is unknown. We evaluated vaccine
105 immunogenicity and efficacy against VOCs in SGH due to the susceptibility of SGH to severe

106 clinical disease, lung pathology, and viral replication in the respiratory tract^{24,25}. SpFN (Fig. 1a)
107 adjuvanted with ALFQ was administered at a high (10 µg) or low dose (0.2 µg), selected based on
108 immunogenicity and efficacy studies of SpFN-ALFQ in mice²⁰, in a either a single (1) and two (2)-
109 vaccination regimen in parallel with 2 injections of phosphate buffered saline (PBS) in control
110 animals (Fig. 1b). Blood for serologic analysis was drawn periodically throughout the study, with
111 key immunogenicity timepoints at weeks 6 and 8 (two and four weeks following last vaccine dose,
112 respectively) and week 11 (seven weeks post final vaccine dose), preceding viral challenge.

113

114 **Strong binding antibody responses elicited by two-dose SpFN-ALFQ vaccination**

115 Robust serum binding antibody responses to the SARS-CoV-2 WA1 spike protein (S-2P) and
116 receptor-binding domain (RBD) were observed at week 6 by ELISA (Fig. 1c). Both the 1- and 2-
117 dose regimens were immunogenic, with higher ELISA titers elicited by the 2-dose regimen against
118 both RBD and spike (S-2P), while responses within regimens did not differ between doses.
119 Endpoint titers against spike (S-2P) at week 6 demonstrated nearly a log difference between
120 dosing regimens, with mean reciprocal dilutions for the 1-dose regimens of 3.2×10^4 (10 µg) and
121 1.92×10^4 (0.2 µg), and 2-dose regimen responses of 1.98×10^5 (10 µg) and 1.35×10^5 (0.2 µg).
122 Endpoint titers did not substantially wane between weeks 6 (Fig. 1c) and 8 (Supplemental Fig. 1a)
123 or week 11 (Fig. 1c), indicating durability of binding antibody responses.

124

125 We then assessed the breadth of post-vaccination binding antibody responses following to WA1
126 and VOCs B.1.1.7 and B.1.351 variant RBD antigens, measured by biolayer interferometry (Fig.
127 1d). Responses again trended higher with the 2-dose regimen and did not differ between the 10

128 μg and 0.2 μg groups within regimens. Binding levels between strains were comparable between
129 WA1 and B.1.1.7 in the 2-dose regimens with B.1.1.7/WA1 mean fold change ratios of 1.02 (10
130 μg) and 1.01 (0.2 μg), while 1-dose group of B.1.1.7/WA1 ratios were 0.88 (10 μg) and 0.82 (0.2
131 μg). Comparatively, B.1.351 cross-reactive binding antibody levels were reduced compared to
132 WA1. B.1.351/WA1 mean fold-change ratios in the 2-dose groups were 0.71 (10 μg) and 0.49 (0.2
133 μg), and in the 1-dose groups 0.29 (10 μg) and 0.14 (0.2 μg). Similar magnitude responses were
134 observed at week 8 (Supplemental Fig. 1b), while binding antibody levels declined by week 11,
135 the time of challenge (Fig 1e). Cross-reactive binding antibodies at week 6 also recognized
136 heterologous B.1.1.7 and B.1.351 cell surface expressed spike protein in a flow cytometric based
137 IgG opsonization assay; responses were consistent with the quantitative differences seen for the
138 inter-group comparisons in Fig. 1 for all three strains (Supplemental Fig. 1c)

139

140 **hACE2 competition and pseudovirus neutralizing antibody responses**

141 As SARS-CoV-2 mediates host cell entry via engagement of the viral spike protein with cell surface
142 expressed human angiotensin-converting enzyme 2 (hACE2) protein, preventing this interaction
143 is a critical target for vaccine induced immune responses²⁶. We measured hACE2 inhibitory
144 antibodies longitudinally using a serum competition assay that detects blockade of RBD-hACE2
145 binding (Fig. 2a). At week 6, mean 50% inhibitory dilution (ID₅₀) values in the 2-dose regimen
146 groups were 145.6 (10 μg) and 106.8 (0.2 μg), and 76.6 (10 μg) and 57.0 (0.2 μg) in the 1-dose
147 groups. Responses did not differ between regimens and were largely stable at week 8 but waned
148 by the time of challenge at week 11.

149

150 Pseudovirus neutralizing antibody responses were measured against the WA1, B.1.1.7 and
151 B.1.351 variants at weeks 6 and 11 (Fig. 2b and Fig. 2c, respectively). At week 6, responses were
152 higher for the 2-dose versus the 1-dose vaccine regimen in most cases (Fig. 2b). Mean log₁₀ ID₅₀
153 values against WA1 ranged from 3.56 (10 µg) to 3.36 (0.2 µg) and 2.88 (10 µg) to 2.17 (0.2 µg) to
154 WA1 in the 2-dose and one-dose regimens, respectively, with comparable titers against B.1.1.7
155 of 3.90 (10 µg), 3.82 (0.2 µg), 2.52 (10 µg) and 2.36 (0.2 µg), respectively. Responses to B.1.351
156 were diminished relative to WA1 and B.1.1.7, notably with the one-dose regimen, with mean
157 log₁₀ ID₅₀ values of 3.46 (10 µg) to 2.74 (0.2 µg) and 1.67 (10 µg) to 1.68 (0.2 µg) in the 2-dose
158 and 1-dose regimens, respectively. Titers were consistently higher for the 2-dose versus the 1-
159 dose vaccine regimen. Neutralizing antibody responses decreased between weeks 6 and 11 and
160 the differences between the 2-dose and 1-dose regimens were less marked (Fig. 2c).
161 Interestingly, cross-neutralization was observed for some animals in the 2-dose regimen against
162 the related sarbecovirus SARS-CoV-1, albeit at reduced levels compared to SARS-CoV-2. Here we
163 demonstrate that SpFN-ALFQ vaccine induces potent neutralization in SARS-CoV-2 VOCs, as well
164 as cross-neutralization against SARS-CoV-1, as previously described in rhesus macaques and
165 mice¹⁸⁻²⁰.

166

167 **Reduction of body-weight loss in SpFN-ALFQ vaccinated, VOCs challenged hamsters**

168 Hamsters were divided into two cohorts comprised of male and female animals and challenged
169 with either B.1.1.7 (n=5) or B.1.351 (n=6) variants of SARS-CoV-2 by intranasal inoculation at
170 week 11, 7 weeks after the last immunization in either the 2-dose or 1-dose vaccine regimen
171 groups. Challenge doses were selected based on prior titration of viral stocks in hamsters,

172 targeting a 10-15% loss of body weight by 7 days post-challenge. Body weight was monitored
173 daily following challenge. For both B.1.1.7 and B.1.351 infection, weight loss of PBS control
174 animals fell as expected between 10-15% by 6 days post-challenge (DPC), with a mean weight
175 loss of 11.6% for B.1.1.7 and 12.7% for B.1.351 respectively (Fig. 3a). For the 10 µg 2-dose
176 vaccinated animals, B.1.1.7 challenged animals had a mean body weight loss of 2.3% and B.1.351
177 challenged animals with slightly higher at 4.0%, but still a dramatic reduction from the PBS
178 vaccinated control hamsters. In the 2-dose vaccine regimen groups, both the 10 µg and 0.2 µg
179 dose groups demonstrated comparable levels of protection, with the one-dose vaccinated
180 animals demonstrating the least protection both for B.1.1.7 and B.1.351 challenges.

181

182 **Undetectable lung and nasal tissue viral load in SpFN-ALFQ vaccinated, viral challenged**
183 **hamsters**

184 To assess the impact of SpFN immunization following challenge by either the B.1.1.7 or B.1.351
185 strains, viral load was assessed by viral culture recovery in lung tissues at day 6 post challenge
186 (Fig. 3b). The mean viral load in the PBS vaccinated control animals challenged with B.1.1.7 was
187 5.67×10^6 TCID₅₀/gram of lung tissue. Virus was not recovered in lung tissue culture in both the
188 10 and 0.2 µg 2-dose and 1-dose vaccine groups (below the limit of detection of 1.78×10^3) (Fig.
189 3b). The mean lung tissue viral load in the PBS control vaccinated animals challenged with B.1.351
190 was 1.36×10^7 TCID₅₀/g. All animals in the 2-dose and 1-dose vaccine groups, for both 10 µg and
191 0.2 µg doses, showed no detectable virus except for one animal in the 10 µg two-dose vaccinated
192 group (Fig. 3b). Viral load was also measured in nasal turbinate tissue collected at day 6 post-
193 challenge, with similar results to lung tissue analysis (Fig. 3c). The mean nasal turbinate tissue

194 viral load in the PBS control vaccinated animals challenged with B.1.1.7 was 1.39×10^6 TCID50/g
195 and B.1.351 was 8.14×10^6 TCID50/g of nasal turbinate, respectively. All vaccinated animals were
196 below the limit of detection (1.492×10^3 TCID50/g), except a single outlier animal in the 0.2 μ g 1-
197 dose vaccination regimen group for B.1.1.7 challenged group, and an outlier animal each in the
198 10 μ g 2-dose and 0.2 μ g 1-dose regimen vaccination groups for B.1.351 challenged animals (Fig.
199 3c). Throughout the challenge phase of the study, oral swabs were collected at days 2, 4 and 6
200 post-challenge and assessed for viral burden by RT-qPCR, by measuring both sub-genomic E
201 messenger RNA (sgmRNA) (Supplemental Fig. 2a and 2c) and total viral RNA (viral load)
202 (Supplemental Fig. 2b and 2d). Overall viral loads decreased modestly over the duration of the
203 challenge in all groups for both B.1.1.7 and B.1.351, with the largest decrease observed at day 6
204 post-challenge in the 2-dose 10 μ g dose vaccination regimen group. These results demonstrate
205 clear protection from tissue viral load in vaccinated animals challenged with B.1.1.7 and B.1.351,
206 a critical determinant in establishing effective vaccines against SARS-CoV-2 VOCs.

207

208 **Lung pathology and tissue nucleocapsid antigen are minimized by SpFN-ALFQ vaccination**

209 Lung pathology was assessed day 6 post-challenge by both routine hematoxylin and eosin (H&E)
210 staining as well as immunohistochemistry (IHC) for the presence of viral nucleocapsid (N) protein
211 (Fig. 4). By semiquantitative scoring of lung histopathology, the highest degree of pathology was
212 seen in the PBS vaccinated control animals challenged with either B.1.1.7 or B.1.351 (Fig. 4a). All
213 PBS vaccinated control animals developed histopathologic evidence of multifocal to extensive,
214 moderate to marked interstitial pneumonia (IP) (Fig. 4b and 4c, for B.1.1.7 and B.1.351 challenged
215 animals, respectively). The pneumonia was characterized by type II pneumocyte hyperplasia,

216 alveolar edema, alveolar inflammatory and necrotic debris, thickening of alveolar septae,
217 bronchiolar epithelial hyperplasia, and increased numbers of pulmonary macrophages (including
218 multinucleated giant cells). The extent of IP present in PBS vaccinated control animals was
219 comparable in animals challenged with either B.1.1.7 or B.1.351. In the B.1.1.7 challenged
220 animals, the least amount of pathology was seen in the animals vaccinated with either 2-dose
221 regimen, although less pathology was evident in all of the SpFN vaccination groups compared
222 with the PBS control group (Fig. 4a - left panel, 4b, 4c and Supplemental Table 1A). For the B.1.351
223 challenged animals, the most protection from lung pathology was observed in the 10 µg, 2-dose
224 vaccine regimen group, although there was a decrease in the mean pathology score of all SpFN
225 vaccinated groups (Fig 4a - right panel, 4b, 4c and Supplemental Table 1A). Overall, there was a
226 trend toward increased pathology observed in the B.1.351 versus the B.1.1.7 animals, in
227 particular with the 1-dose groups. In the 10 µg 2-dose group however, protection between VOCs
228 were comparable. Immunohistochemistry demonstrated strong, multifocal to focally extensive
229 (>500-1000 cells per section) immunopositivity to SARS-CoV-2 nucleocapsid (N) protein in
230 bronchiolar epithelium, alveolar pneumocytes and pulmonary macrophages in the lungs of all
231 unvaccinated animals. Viral antigen detected in lung sections from animals in the 10 µg and 0.2
232 µg vaccine groups was substantially reduced compared with the PBS vaccinated groups with the
233 greatest reduction seem in the 10 µg 2-shot vaccine groups (Supplemental Table 1B). Taken
234 together, SpFN adjuvanted with ALFQ confers clear protection from viral burden and pathology
235 in the lungs following VOC challenge.

236

237 **Discussion**

238 The development of effective and safe vaccines in response to the SARS-CoV-2 pandemic has
239 occurred at an unprecedented rate. This success has been tempered by the reduced vaccine
240 efficacy against some emerging VOCs, most notably B.1.351^{4,5,8,11,13,16,27}. The need for more
241 broadly effective vaccines against multiple lineages of SARS-CoV-2 will likely increase, as
242 underscored by the rapid rise of VOCs in India, including B.1.1.7 and emerging variants B.1.617
243 with derivative lineages, and B.1.618³. As B.1.1.7 has become the dominant variant in the U.S.²⁸
244 and B.1.351 and B.1.617 lineages are becoming more dominant in many areas of the world,
245 evaluation of existing and novel vaccines against these strains is essential. As the pandemic
246 continues, SARS-CoV-2 will not only adapt to replicate more efficiently in the human host and
247 evolve to escape host immune responses to natural infection, it will increasingly adapt to vaccine
248 evoked immune responses. This large number of products administered globally, with differential
249 vaccine efficacy, will further drive the evolution of virus variants that may be more resistant to
250 current formulations of SARS-CoV-2 vaccines. This will be especially true in populations where
251 immunocompromised individuals are prevalent (e.g., HIV infection, cancer therapies, organ
252 transplant, autoimmune diseases) providing an ideal milieu for the generation of virus variants
253 to challenge current and next generation SARS-CoV-2 vaccines²⁹.

254

255 We evaluated the efficacy of a novel vaccine, currently in clinical trials (ClinicalTrials.gov
256 Identifier: NCT04784767), against VOCs. SpFN adjuvanted with ALFQ, has been previously
257 demonstrated to be highly efficacious against the WA1 strain of SARS-CoV-2 in nonhuman
258 primate and murine models^{17,18,20}. In this study, sera from hamsters that were immunized at 10
259 μg and 0.2 μg doses as 1- and 2-dose regimens demonstrated dose-dependent binding,

260 neutralizing and hACE2 inhibiting antibody activity, with the highest responses seen in the 2-dose
261 regimens. The strongest responses against WA1, B.1.1.7 and B.1.351 were observed in the 10 µg
262 group using a 2-dose regimen, with similar binding responses observed between WA1 and
263 B.1.1.7, that were reduced slightly against B.1.351 in the 10 µg, 2-dose regimen but more
264 substantially in the 1-dose regimens. Humoral immunity waned from peak responses at study
265 weeks 6 and 8 to the time of challenge at week 11. Opsonizing IgG responses, shown to be
266 associated with protection against SARS-CoV-2 in small-animal models, were also elicited³⁰⁻³⁴.
267 Additionally, prior studies have demonstrated that vaccine-induced antibody Fc-mediated
268 functions are also associated with protection against SARS-CoV-2³⁵⁻³⁷. Here, we demonstrated
269 that the SpFN vaccine was able to elicit high IgG opsonization against both wild type and VOCs in
270 hamsters, suggesting that SpFN-ALFQ vaccine induced antibodies that could leverage Fc-
271 mediated functions associated with protection from SARS-CoV-2 VOCs to include B.1.351. Of
272 note, we observed strong neutralizing responses in the 10 µg, 2-dose regimen groups that were
273 similar across WA1, B.1.1.7 and B.1.351 variants. This is particularly encouraging as many studies
274 have demonstrated decreased neutralizing antibody responses of convalescent or vaccinee sera,
275 in particular against B.1.351^{4,11,14,16,27}. hACE2-RBD binding inhibition levels mirrored overall
276 humoral responses. This assay has functional implications for cellular entry and in conjunction
277 with the binding and neutralization assays, will be critical to utilize in future studies to understand
278 the critical correlates of protection conferred during SpFN-ALFQ vaccination in SGH and NHP
279 models.
280

281 As expected from the humoral responses, mitigation of body weight loss was also observed in
282 vaccinated animals, following SARS-CoV-2 VOC challenge, most dramatically in the 2-dose
283 vaccinated animals. Hamsters were challenged with doses of B.1.1.7 or B.1.351 targeted to result
284 in a 10-15% loss of body weight in control animals. In the 2-dose regimen at both 10 μ g and 0.2
285 μ g doses for B.1.1.7, loss of bodyweight was dramatically reduced, from ~12% observed in the
286 PBS control animals to between 2-3% in the vaccinated groups. Notably, a single vaccination in
287 the 10 μ g dose group was also sufficient to confer similar protection, with the even low-dose
288 conferring intermediate levels of protection after a single immunization. In the case of B.1.351,
289 protection in the prime-boost regimen had a similar range of protection, from the ~13%
290 bodyweight loss observed in the PBS treated animals to 3-4%. Single-doses were less protective
291 than observed for B.1.1.7 challenge, but still conferred intermediate protection against B.1.351
292 challenge. These results are highly encouraging, showing potential protective efficacy of the
293 SpFN-ALFQ vaccine against clinical disease caused by VOC to include B.1.351, particularly using a
294 2-dose regimen.

295

296 Following the challenge phase of the study, assessment of viral loads by TCID50 in lung tissues
297 and nasal turbinate demonstrated clear protection from challenge with either B.1.1.7 or B.1.351,
298 with complete elimination of recoverable virus detected in the majority of animals, regardless of
299 vaccine regimen, by day 6 post challenge. Adjunctive analysis of oral swab viral load, either total
300 RNA or subgenomic mRNA, products of discontinuous SARS-CoV-2 transcription only seen during
301 active viral replication, confirmed the lung and nasal turbinate tissue viral culture data in showing
302 virologic evidence of SpFN-ALFQ protection with either B.1.1.7 or B.1.351 challenge.

303

304 A key question that this study was designed to address through the utilization of SGH as a
305 pathogenic model of SARS-CoV-2 disease, was whether SpFN-ALFQ had an impact on lung
306 pathology developed during acute infection with B.1.1.7 or B.1.351. Challenge doses of B.1.1.7
307 and B.1.351 utilized in this study gave nearly equivalent pathology in unvaccinated (PBS) control
308 animals, with significant type II pneumocyte hyperplasia and cellular infiltrate occurring within
309 the lung on H&E, and viral staining observed by detection of viral nucleocapsid (N) protein by
310 immunohistochemistry. For B.1.1.7 challenged animals, pathology was dramatically reduced in
311 both the high and low-dose prime-boost groups. 1-dose 10 µg and 0.2 µg vaccine regimens
312 conferred intermediate levels of protection, with wider variability in individual pathology within
313 individuals. In the B.1.351 challenged animals, the 10 µg 2-dose vaccine regimen also
314 demonstrated decreases in pathology compared with the cognate PBS control, with intermediate
315 levels of protection conferred to the 0.2 µg groups. Taken together, SpFN-ALFQ generated robust
316 binding antibody and neutralizing antibody responses in SGH against WA1, B.1.1.7 and B.1.351
317 SARS-CoV-2 variants. It was also protective in intranasal challenge with the B.1.1.7 and B.1.351
318 variants as assessed by body weight preservation, lung tissue viral load, oral fluid total and
319 sgmRNA, and standard histopathological and immunohistochemical analysis of lung tissues at
320 necropsy.

321

322 Publically available preprint reports have recently shown that the vaccines being marketed by
323 AstraZeneca, ChAdOx1 nCoV-19 (AZD1222), and Moderna, mRNA-1273, show protection against
324 B.1.351 challenge in hamster and rhesus models, respectively^{27,38}. Another preprint describes

325 protection from B.1.351 challenge in human ACE2 transgenic mice vaccinated with the CureVac
326 mRNA vaccine, CVnCoV³⁹. Continued molecular epidemiologic analysis of ongoing SARS-CoV-2
327 infections with concomitant assessment of the impact of emerging VOCs on current and next-
328 generation SARS-CoV-2 vaccines will be essential for achieving and maintaining pandemic
329 control, and underpins the scientific approach to both pan-SARS-CoV-2 and pan-coronavirus
330 vaccine research and development. To this end, SpFN-ALFQ is now being evaluated in a first in
331 human phase I clinical trial as a platform approach toward broader application to the
332 betacoronavirus genus and the entire family of coronaviruses.

333

334 **Methods**

335

336 **Transfection, Expression and Purification of SpFN 1B-06-PL**

337 Expi293 cells (Gibco, Cat No. A14527) were maintained and passaged as per manufacturer's
338 guidelines in Expi293 Expression Media (Gibco, Cat No. A1435101) at 37°C, 8% CO₂, 120 RPM, ≥
339 60% RH. Briefly, the transfection reaction consisted of 1mg of purified, cGMP sourced plasmid
340 DNA (Aldevron, pCoV 1B-06-PL) plus 3mL of Turbo 293 Transfection Reagent (Speed Biosystems,
341 Cat No. PXX1001) mixed in 1X PBS per liter of transfected cells. The reaction was incubated at 20-
342 25°C for 15 minutes and 125mL/flask was rapidly and aseptically transferred to 16 single use 3L
343 Erlenmeyer shake vented flasks (Corning, Cat no. 431252) each containing 1.125L of Expi293 cells
344 passaged at a density of 2.0 x 10⁶ cells/ml on the day of transfection. After the addition of the
345 transfection reaction, the transfected cells were incubated at 34°C, 8% CO₂, 120 RPM, ≥ 60% RH
346 for 5 days. The expressed product was collected, clarified by double centrifugation at 4000 RPM,

347 10°C, for 30 minutes, followed by depth filtration (0.65µM + 0.45µM, Sartorius, Sartobran P, Cat
348 No. 5235306D0-SO-V) and stored at 2-8°C for further downstream processing.

349

350 SpFN 1B-06 PL was purified, concentrated and dialyzed against 50 mM Tris, 50mM NaCl, pH 8.0
351 solution. Briefly, 16 L of clarified expression product was initially concentrated 6 fold using a
352 tangential flow filtration module (500 kD MW Cutoff, mPES MiniKros, Cat No.N04-500-05). The
353 concentrate was treated with Benzonase (EMD Millipore, Cat No.EM1.01695.0001) for 120min
354 at 22°C before conducting a buffer exchange into 50 mM Tris, 50mM NaCl, pH 7.915. The material
355 was loaded onto a 4.4 x 14 cm Fractogel DEAE (M) Column (EMD Millipore, Cat No.1168835000)
356 with a bed volume of 212 mL. SpFN 1B-06 PL bound to the column and was eluted with 50 mM
357 Tris Base, 200 mM NaCl, pH 8.018, 21.55 mS/cm. Following this, a 44 mL Capto Core 400 column
358 (Cytiva, Cat No.17372403) was used as a polishing step to remove any potential lower MW
359 contaminants. A final dialysis step was performed to place the product into the final formulation
360 buffer using a 300 kD MWCO UF cartridge (Repligen mPES MiniKros, Cat No. S02-E300-05). The
361 final purified SpFN 1B-06 PL recovery yielded 55.47 mg in a volume of 215 mL, approximately a
362 3.47 mg/L yield from the cell expansion and growth.

363

364 **Viral stock propagation and preparation**

365 B.1.1.7 viral stocks were generated from seed stock (USA/CA_CDC_5574/2020), obtained from
366 BEI resources (Cat # NR-54011, Lot # 70041598) and expanded in Calu-3 cells (incubated at 37°C
367 for 3 days). The viral stock lot used for this study (Lot # 012921-1230) was titrated in Vero-
368 TMPRSS2 cells, with viral titers of 1.375×10^6 PFU/mL. This stock was used undiluted for viral

369 challenge with 100 μ L intranasally, for a final challenge concentration of 1.375×10^5 PFU/mL per
370 dose.

371

372 B.1.351 viral stocks were propagated and characterized by deep sequencing as previously
373 described³⁸. Briefly, hCoV-19/USA/MD-HP01542/2021 (B.1.1.351) was derived from the seed
374 stock (Lot# MD-HP JHU P2) and propagated in in VeroE6-TMPRSS2 cells. The viral titer of the
375 B.1.351 stock used for this study was 3×10^7 PFU/ml in VeroE6-TMPRSS2 cells, diluted 1:100 in
376 PBS for a challenge dose of 3×10^4 PFU in 100 μ L.

377

378 **Syrian golden hamster immunizations**

379 Male and female Syrian golden hamsters (6-8 week-old, n = 55) were acquired from Charles River
380 Laboratories and housed at Bioqual, Inc., for the duration of the study. Following one week of
381 acclimatization, animals were immunized intramuscularly in caudal thighs with PBS (control) or
382 SpFN immunogen of differing doses (10 μ g or 0.2 μ g) pre-formulated with a fixed dose of ALFQ
383 (20 μ g of 3D-PHAD (monophosphoryl 3-deacyl lipid A (synthetic)) and 10 μ g of QS21)⁴⁰. The
384 design, production, stability, and initial characterization of SpFN adjuvanted with ALFQ has been
385 described previously²⁰. Briefly, the immunogen is based on the Spike protein of the WA1 SARS-
386 CoV-2 variant with S-2P amino acid modifications expressed as a fusion protein with H. pylori
387 ferritin in mammalian cells that self-assembles into an ordered nanoparticle each of which
388 presents 8 Spike trimers. SpFN was formulated with ALFQ prior to administration. SpFN was
389 produced at the WRAIR Pilot Bioproduction Facility in October 2020 as an engineering batch and
390 stored at 4°C for 3-4 months for the prime and boost/single immunization doses, respectively.

391 Boosting immunizations were injected contralaterally from the prime four weeks following the
392 prime. In-life blood sampling was conducted by retro-orbital bleeds. Maximum blood collections
393 were determined based on animal weight and frequency of collection, in consultation with
394 veterinary guidance. Following collections, animals were monitored until fully recovered from
395 the anesthetic and the procedure.

396

397 **SARS-CoV-2 Syrian golden hamster challenge**

398 Animals were challenged with SARS-CoV-2 seven weeks following the boost or single
399 immunization. Animals were anesthetized with ketamine/xylazine and challenged by intranasal
400 inoculation of 50 μ L virus in each nostril in a drop-wise manner (100 μ L/hamster). Challenge dose
401 was pre-determined for each VOC viral stock to achieve comparable clinical disease as manifested
402 by body weight loss of 10-15%. B.1.1.7 virus was administered at a challenge dose of 1.375×10^5 .
403 B.1.351 virus was administered at a challenge dose of 3×10^4 PFU per hamster. Following viral
404 challenge, all animals were weighted and observed twice daily for clinical signs (ruffled fur,
405 hunched posture, behavior, etc.), with euthanasia criteria of 20% loss of pre-challenge body
406 weight or becoming moribund. At study termination 6 DPC, all animals were terminally
407 anesthetized by ketamine/xylazine, followed by exsanguination by cardiac puncture (for terminal
408 blood collection) and euthanasia. Tissues were collected for use in downstream virologic,
409 immunologic, molecular and histopathology studies. Animals were housed in BLS-2 during the
410 vaccination phase and BSL-3 facilities during the challenge phase.

411

412 **Enzyme Linked Immunosorbent Assay (ELISA)**

413 96-well Immulon “U” Bottom plates were coated with 1 µg/mL of RBD or S protein (S-2P) antigen
414 in Dulbecco’s PBS, pH 7.4. Plates were incubated at 4°C overnight and blocked with blocking
415 buffer (PBS containing 0.5% Casein and 0.5% BSA, pH 7.4), at room temperature (RT) for 2 h.
416 Individual serum samples were serially diluted 2-fold in blocking buffer and added to triplicate
417 wells and the plates were incubated for 1 hour at RT. The plates were washed with PBS containing
418 0.1% Tween 20, pH 7.4, followed by the addition of horseradish peroxidase (HRP)-conjugated
419 goat anti-Hamster IgG (H+L) (1:2000 dilution) (SouthernBiotech) for an hour at RT. The HRP
420 substrate, 2,2'-Azinobis [3-ethylbenzothiazoline-6-sulfonic acid]-diammonium salt (ABTS) (KPL)
421 was added to the plates for 1 hour at RT. The reaction was stopped by the addition of 1% SDS per
422 well and the absorbance (A) was measured at 405 nm (A405) using an ELISA reader Spectramax
423 (Molecular Devices, San Jose, CA) within 30 min of stopping the reaction. The results are
424 expressed as end point titers, defined as the reciprocal dilution that gives an absorbance value
425 that equals twice the background value (antigen-coated wells that did not contain the test sera,
426 but had all other components added).

427

428 **Biolayer Interferometry RBD binding assay**

429 All biosensors were hydrated in PBS prior to use. All assay steps were performed at 30°C with
430 agitation set at 1,000 rpm in the Octet RED96 instrument (FortéBio). HIS1K biosensors (FortéBio)
431 were equilibrated in assay buffer (PBS) for 30 seconds before loading of His-tagged SARS-CoV-2
432 WA1 RBD or VOC RBDs B1.1.7, and B.1.351 (30 µg/mL diluted in PBS) for 120 seconds.
433 Immobilized RBD proteins were then dipped in hamster sera (100x dilution with PBS) for 180
434 seconds followed by dissociation for 60 seconds. Binding response values were recorded at 180

435 seconds. SARS-CoV-2 RBD constructs (residues 331 - 527), modified to incorporate a N-terminal
436 hexa-histidine tag (for purification), were derived from the Wuhan-Hu-1 strain genome
437 sequence (GenBank MN9089473) and synthesized and subcloned into a CMVR plasmid by
438 Genscript. RBD with VOC point mutations were generated using a modified QuikChange site-
439 directed mutagenesis protocol (Agilent). The constructs resulting from site-directed mutagenesis
440 were amplified and isolated from *E. coli* Stbl3 or Top10 cells. Large-scale DNA isolation was
441 performed using either endo free Maxiprep, Megaprep or Gigaprep kits (Qiagen). All expression
442 plasmids were transiently transfected into Expi293F cells (Thermo Fisher Scientific) using
443 ExpiFectamine 293 transfection reagent (Thermo Fisher Scientific). Cells were grown in
444 polycarbonate baffled shaker flasks at 34°C and 8% CO₂ at 120 rpm. Cells were harvested 5-6 days
445 post-transfection via centrifugation at 3,500 x g for 30 minutes. Culture supernatants were
446 filtered with a 0.22-µm filter and stored at 4°C prior to purification. His-tagged RBD proteins were
447 purified using Ni-NTA affinity chromatography, with 1 mL Ni-NTA resin (Thermo Scientific) used
448 to purify protein from 1L of expression supernatant. Ni-NTA resin was equilibrated with 5 column
449 volumes (CV) of phosphate buffered saline (PBS) (pH 7.4) followed by supernatant loading 2 x at
450 4°C. Unbound protein was removed by washing with 200 CV of PBS, followed by 50 CV 10mM
451 imidazole in PBS. Bound protein was eluted with 220 mM imidazole in PBS. All proteins were
452 further purified by size-exclusion chromatography using a 16/60 Superdex-200 purification
453 column. Purification purity for all the proteins was assessed by SDS-PAGE.

454

455 **Biolayer Interferometry hACE2 competition assay**

456 All biosensors were hydrated in PBS prior to use. All assay steps were performed at 30°C with
457 agitation set at 1,000 rpm in the Octet RED96 instrument (FortéBio). SARS-CoV-2 RBD - hACE2
458 competition assays were carried out as follows. SARS-CoV-2 RBD (WA1 strain, 30 µg/ml diluted
459 in PBS) was immobilized on HIS1K biosensors (FortéBio) for 180 seconds followed by baseline
460 equilibration for 30 seconds. Serum binding was allowed to occur for 180 seconds followed by
461 baseline equilibration (30 seconds). Recombinant hACE2 protein (30 µg/ml) was then allowed to
462 bind for 120 seconds. Percent inhibition (PI) of hACE2 binding to the RBD by serum was
463 determined using the equation: $PI = 100 - ((hACE2 \text{ binding in the presence of mouse serum} /$
464 $hACE2 \text{ binding in the absence of mouse serum}) \times 100)$.

465

466 **IgG Opsonization Assays**

467 SARS-CoV-2 S-expressing expi293F cells were generated by transfection with linearized plasmid
468 (pcDNA3.1) encoding codon-optimized full-length SARS-CoV-2 S protein matching the amino acid
469 sequence of the IL-CDC-IL1/2020 isolate (GenBank ACC# MN988713), the B.1.1.7 isolate⁹, or the
470 B.1.351 isolate⁴¹. Stable transfectants were single-cell sorted and selected to obtain a high-level
471 Spike surface expressing clone (293F-Spike-S2A). 293F-Spike-S2A cells were incubated with 100
472 µl of plasma diluted 100-fold in RPMI containing 10% FBS (R10) for 30 minutes at 37°C. Cells were
473 washed 3 times and stained with a goat anti-hamster IgG (H+L) Alexa Fluor 488 (ThermoFisher
474 Scientific). Cells were then fixed with 4% formaldehyde solution and fluorescence was evaluated
475 on a LSRII analytic cytometer (BD Bioscience).

476

477 **SARS-CoV-1 and SARS-CoV-2 pseudovirus neutralization assay**

478 Pseudovirions were produced by co-transfection of HEK293T/17 cells with either the SARS-CoV-
479 1 (Sino 1-11, GenBank # AY485277) or SARS-CoV-2 (WA1/2020 GenBank # MT246667) S
480 expression plasmid and an HIV-1 pNL4-3 luciferase reporter plasmid (pNL4-3.Luc.R-E-, NIH AIDS
481 Reagent Program). The S expression plasmid sequences for SARS-CoV-2 and SARS-CoV-1 were
482 codon optimized and modified to remove an 18 amino acid endoplasmic reticulum retention
483 signal in the cytoplasmic tail in the case of SARS-CoV-2, and a 28 amino acid deletion in the
484 cytoplasmic tail in the case of SARS-CoV-1 to improve S incorporation into pseudovirions and
485 improve infectivity. S expression plasmids for SARS-CoV-2 VOC were similarly codon optimized,
486 modified and included the following mutations: B.1.1.7 (69-70del, Y144del, N501Y, A570D,
487 D614G, P681H, T718I, S982A, D1118H), B.1.351 (L18F, D80A, D215G, 241-243del, K417N, E484K,
488 N501Y, D614G, A701V, E1195Q). Virions pseudotyped with the vesicular stomatitis virus (VSV) G
489 protein were used as a non-specific control. Infectivity and neutralization titers were determined
490 using ACE2-expressing HEK293 target cells (Integral Molecular). Test sera were diluted 1:40 in
491 cell culture medium and serially diluted; then 25 μ L/well was added to a white 96-well plate. An
492 equal volume of diluted SARS-CoV-2 PSV was added to each well and plates were incubated for
493 1 hour at 37°C. Target cells were added to each well (40,000 cells/ well) and plates were
494 incubated for an additional 48 hours. Relative light units (RLU) were measured with the EnVision
495 Multimode Plate Reader (Perkin Elmer, Waltham, MA) using the Bright-Glo Luciferase Assay
496 System (Promega, Madison, WI). Neutralization dose–response curves were fitted by nonlinear
497 regression using the LabKey Server. Final titers are reported as the reciprocal of the dilution of
498 serum necessary to achieve 50% (ID₅₀, 50% inhibitory dose). Assay equivalency for SARS-CoV-2
499 was established by participation in the SARS-CoV-2 Neutralizing Assay Concordance Survey

500 (SNACS) run by the Virology Quality Assurance Program and External Quality Assurance Program
501 Oversight Laboratory (EQAPOL) at the Duke Human Vaccine Institute, sponsored through
502 programs supported by the National Institute of Allergy and Infectious Diseases, Division of AIDS.
503

504 **Oral cavity viral RNA measurements**

505 The oral cavity was swabbed with a sterile flocked swab that was immediately placed into a
506 cryovial with 1mL PBS. Vials were snap-frozen on dry ice and stored at -80°C until testing. Viral
507 RNA was extracted from 200 ul of oral swab material using the Qiagen EZ1 DSP Virus kit on the
508 automated EZ1 XL Advance instrument (Qiagen, Valencia, CA). Real-time quantitative reverse
509 transcription – polymerase chain reactions (RT-qPCR) were performed on the 7500 Dx Fast
510 thermal cycler (Thermo Fisher Scientific, Life Technologies, Carlsbad, CA). SARS-CoV-2 specific
511 forward and reverse primers and probe targeting the E gene encoding the envelope protein were
512 used for amplification of the viral RNA. Amplification of the sgmRNA was achieved using the
513 Leader TRS sequence specific primer, the reverse E primer and the E specific probe as described
514 previously¹⁸. A synthetic RNA for subgenomic E was used as a calibrator. Final results were
515 reported in copies/ml.

516

517 **Tissue viral burden by TCID50**

518 The infectious titer determination from lungs and nasal turbinates was obtained by performing
519 a TCID50 assay. Vero TMPRSS2 cells were plated at 25,000 cells per well in DMEM
520 supplemented with 10% FBS and gentamicin. Cells were incubated at 37°C, 5.0% CO₂. When
521 cells achieved 80-100% confluency, the media was aspirated and replaced with 180µL of DMEM

522 containing 2% FBS and gentamicin. 0.10-0.20 mg sections of the right lobe of the lung and the
523 nasal turbinates were collected at necropsy, snap frozen, and stored at -80°C until processing.
524 Frozen tissue was placed in 15 mL conical tube on wet ice containing 0.5 mL media and
525 homogenized 10-30 secs (Probe, Omni International: 32750H). The tissue homogenate was
526 spun to remove debris at 2000 *g*, 4°C for 10 min. The supernatant was then passed through a
527 strainer (Pluriselect: Cat No. 43-10100-40) into the original vial and kept on wet ice. From the
528 strained supernatant, 20 µL aliquots were tested in quadruplicate in a 96-well plate format. The
529 top row of the 96-well plate was mixed 5 times and serially diluted by pipette transfer of 20 µL,
530 representing 10-fold dilutions. Pipette tips were disposed of between each row and mixing was
531 repeated until the last row on the plate. After incubation for 4 days, wells were visually
532 inspected for cytopathic effects (CPE) scored as CPE minus (-) where non-infected wells have a
533 clear confluent cell layer, or CPE plus (+), where rounding of infected cells is observed. Positive
534 controls were utilized for optimal assay performance, where the TCID₅₀ tested within 2-fold of
535 the expected value. TCID₅₀ of all samples were calculated using the Read-Muench formula.

536

537 **Histology and immunohistochemistry**

538 Lungs from 6 DPC were insufflated and perfused with 10% neutral-buffered formalin. Three
539 tissue sections from each of the left lung lobes were used to evaluate the lung
540 pathology. Sections were processed routinely into paraffin wax, then sectioned at 5 µm, and
541 resulting slides were stained with hematoxylin and eosin. Immunohistochemistry (IHC) on
542 formalin fixed paraffin embedded tissue sections was performed using the Dako Envision system
543 (Dako Agilent Pathology Solutions, Carpinteria, CA, USA). Briefly, after deparaffinization,

544 peroxidase blocking, and antigen retrieval, sections were stained with an anti-SARS-CoV/SARS-
545 COV-2 nucleocapsid (N) protein rabbit monoclonal antibody (#40143-R001, Sino Biological,
546 Chesterbrook, PA, USA) at a dilution of 1:6000 and incubated at RT for 45 min. Sections were
547 rinsed and stained with peroxidase-labeled polymer (secondary antibody) for 30 min. Slides were
548 rinsed and a brown chromogenic substrate 3,3' Diaminobenzidine (DAB) solution (Dako Agilent
549 Pathology Solutions) was applied for 8 min. Slides were rinsed, counterstained with hematoxylin,
550 and rinsed. The sections were dehydrated, cleared with Xyless II, and cover-slipped. All tissue
551 slides were evaluated by a board-certified veterinary anatomic pathologist blinded to study
552 group allocations. Semi-quantitative scoring of pulmonary pathology was performed, with
553 grading of intra-alveolar edema, type II pneumocyte hyperplasia, mononuclear cellular infiltrates,
554 polymorphonuclear cellular infiltrates, alveolar histiocytosis, alveolar necrosis, bronchioalveolar
555 epithelial degeneration, bronchiolar epithelial hyperplasia, and interstitial collagenous
556 deposition. Each finding was scored as follows: 0 - absent, 1 - minimal (<10% of tissue section
557 affected); 2 - mild (11-25% of tissue section affected); 3 - moderate (26-50% of tissue section
558 affected); 4 - marked (51-75% affected); 5- severe (>75% of tissue section affected). IHC sections
559 were examined at 400X magnification and evaluated for the number of immunopositive cells per
560 slide.

561

562 **Ethical Statement**

563 All animal *in vivo* procedures were carried out in accordance with institutional, local, state, and
564 national guidelines and laws governing research in animals including the Animal Welfare Act.
565 Animal protocols and procedures were reviewed and approved by the Animal Care and Use

566 Committee of both the US Army Medical Research and Development Command (USAMRDC)
567 Animal Care and Use Review Office as well as the Institutional Animal Care and Use Committee
568 of Bioqual, Inc. (protocol number 20-144). Bioqual, Inc. and the USAMRDC are accredited by the
569 Association for Assessment and Accreditation of Laboratory Animal Care and are in full
570 compliance with the Animal Welfare Act and Public Health Service Policy on Humane Care and
571 Use of Laboratory Animals. Oversight of all research was approved and conducted by the
572 WRAIR Institutional Biological Safety Committee.

573

574 **Statistical Analysis**

575 All statistical analysis were performed using GraphPad Prism version 8 software. All statistical
576 tests shown were performed using the Kruskal-Wallis test with Dunn's correction, comparing all
577 variables (multiple comparison analysis, not against a standard control). Actual p-values for
578 each comparison annotated for statistically relevant values, or for values near statistical
579 significance. All other not statistically or biologically relevant values reported as not-significant
580 (ns). Comparisons to PBS control group are shown directly above each vaccine treatment
581 condition (gray), with inter/intra vaccine regimen comparisons indicated by a solid line between
582 groups, with the statistical result directly above (black).

583

584 **Figure Legends**

585 **Figure 1. Antibody responses following SpFN-ALFQ immunization. a,** The 3-dimensional model
586 of SpFN with Spike protein trimers (green) decorating a ferritin core (gray) as viewed down a 3-
587 fold axis. **b,** Experimental design with hamsters receiving immunization at weeks 0 and 4 in the
588 2-dose regimen and week 4 in the 1-dose regimen as depicted by green SpFN structures above
589 the time-line and check marks below the timeline indicating immunogen dose (10 µg or 0.2 µg
590 or PBS control). Phlebotomy samples were taken at weeks 0, 6, 8 and 11 as indicated by red
591 arrows. Intranasal (IN) viral challenge was performed at week 11 with either VOC B.1.1.7 or
592 B.1.351 viral stocks with the number of animals challenged noted parenthetically. Oral swabs
593 were collected at 2, 4, and 6 days post challenge (DPC) as indicated by blue arrows above the
594 timeline. Necropsy was performed on all animals at day 6 post-challenge as indicated by the black
595 arrow. **c,** ELISA was performed using either WA1 derived Receptor Binding Domain (RBD) or S-2P
596 Spike proteins from sera taken at weeks 6 and 11. Sera from week 0 was also assessed, with no
597 detectable signal observed in any samples (data not shown). The vaccine regimens are indicated
598 on the x-axis by PBS (control) or SpFN dose with the number of vaccinations in the regimen given
599 parenthetically and by color code (blue, 2-dose, red, 1-dose). Endpoint titers are given on the y-
600 axis as geometric mean titers with data displayed in box plots with the top and bottom bars of
601 the box the standard deviation and the middle bar as the median value. P-values for active
602 vaccination groups compared with PBS control are given just above the boxes in light grey while
603 intra-active regimen p-values are given above the boxes in black. ns, not significant ($p > 0.05$)
604 using the Kruskal-Wallis multiple comparisons test, with Dunn's correction. **d,e,** Octet Biolayer
605 Interferometry (BLI) responses against the WA1, B.1.1.7, and B.1.351 sequences of the RBD are

606 given for the vaccination regimens as in C on the x-axis at weeks 6 (**d**) and 11 (**e**). BLI responses
607 are given in nanometers (nm) on the y-axis. Color coding and statistical treatments are as in **c**.

608

609 **Figure 2. Human angiotensin-converting enzyme competition and pseudovirus neutralization**

610 **responses following SpFN-ALFQ immunization. a,** Human angiotensin-converting enzyme

611 competition (hACE2) assays were performed from sera taken at week 6, 8, and 11. The vaccine

612 regimens are indicated on the x-axis by PBS (control) or SpFN dose with the number of

613 vaccinations in the regimen given parenthetically and by color code (blue, 2-dose, red, 1-dose).

614 Inhibitory dose 50% (ID50) are given on the y-axis as with data displayed in box plots with the top

615 and bottom bars of the box the standard deviation and the middle bar as the median value. P-

616 values for SpFN-ALFQ vaccination groups compared with PBS control are given just above the

617 boxes in light grey while intra-active regimen p-values are given above the boxes in black. ns, not

618 significant ($p > 0.05$) using the Kruskal-Wallis multiple comparisons test, with Dunn's correction.

619 **b,c,** Pseudovirus neutralization at weeks 6 and 11 are given against Spike proteins derived from

620 WA1, B.1.1.7, B.1.351 SARS-CoV-2 variants and from SARS-CoV-1. The vaccine regimens are

621 indicated on the x-axis as in **a**. The neutralization titers are given as inhibitory dose 50% (ID50)

622 on the y-axis which is a logarithmic scale. The data are given as box plots and statistically treated

623 as described in **a**.

624

625 **Figure 3. Body weight changes and lung viral load post-challenge.** Daily weights were gathered

626 on hamsters from the time of viral challenge to necropsy on day 6 post challenge when lungs

627 were harvested for a whole tissue, culture based viral load assessment in Vero TMPRSS2 cells. **a,**

628 Mean percent body weight changes plus and minus standard error of the mean (SEM) are given
629 on the y-axis for groups of hamsters assigned to phosphate buffered saline control (PBS) or SpFN-
630 ALFQ vaccination from day of challenge (day 0) to day of necropsy (day 6) for either B.1.1.7 or
631 B.1.351 challenge. Data from immunization groups are given in each graph as PBS (grey plot,
632 phosphate buffered saline control) or active immunogen dose (blue circle/ blue solid line, 10 μ g
633 2-dose regimen; black triangle/ blue dotted line, 0.2 μ g 2-dose regimen; red circle/red solid line,
634 10 μ g 1-dose regimen; black triangle/red dotted line, 0.2 μ g 1-dose regimen. Number of
635 vaccinations in the vaccine regimen are also given parenthetically within each graph. **b**, SARS-
636 CoV-2 viral load data from lung tissue harvested on day 6 post challenge is given on the y-axis as
637 the tissue culture infective dose, 50% (TCID50) per gram of tissue as titered on Vero TMPRSS2
638 cells and read out by cytopathic effects for either B.1.1.7 and B.1.351 challenged hamsters.
639 Immunization groups are given on the x-axis as PBS (phosphate buffered saline) control (gray
640 circles); 10 μ g and 0.2 μ g 2-dose vaccine regimens (blue circles); 10 μ g and 0.2 μ g 1-dose vaccine
641 regimens (red circles). Group data are plotted with the median group value given by the middle
642 bar of the box plot. The dotted horizontal line is the lower limit of detection of the assay. **c**, SARS-
643 CoV-2 viral load data from nasal turbinate tissue harvested on day 6 post challenge is given as in
644 **b**. **b**, **c**, P-values for SpFN-ALFQ vaccination groups compared with PBS control are given just
645 above the boxes in light grey while intra-active regimen p-values are given above the boxes in
646 black. ns, not significant ($p > 0.05$) using the Kruskal-Wallis multiple comparisons test, with
647 Dunn's correction.

648

649 **Figure 4. Standard and immunohistopathologic examination post-challenge.** Lung tissues were
650 collected at necropsy on day 6 post-challenge, fixed with neutral buffered formalin, and stained
651 with hematoxylin and eosin (H&E) for standard microscopic examination as well as submitted
652 for immunohistochemical (IHC) staining for SARS-CoV-2 nucleocapsid (N) protein. **a**, H&E stained
653 slides were scored for pathologic effects on the y-axis (see Methods) for B.1.1.7 (left) and B.1.351
654 (right) challenged hamsters. Vaccination groups were plotted in box plots where the horizontal
655 bar is the median group score. Vaccination groups are given as: PBS (phosphate buffered saline)
656 control (gray circles); 10 µg and 0.2 µg 2-dose vaccine regimens (blue circles); 10 µg and 0.2 µg
657 1-dose vaccine regimens (red circles). **b,c**, Representative lung tissue sections from the PBS
658 control and 10 µg and 0.2 µg 2-dose and 1-dose regimens with the number of vaccinations given
659 parenthetically for B.1.1.7 (**b**) and B.1.351 (**c**) challenged hamsters in the columns as indicated.
660 Rows are given by either H&E at 10- and 200-times magnification power (10X and 200X,
661 respectively) or IHC of SARS-CoV-2 viral antigen at 100 times magnification power (100X). The
662 black boxes in the top row indicate the area magnified in the middle row. Interstitial pneumonia
663 is characterized by inflammatory cellular infiltrates (triangle), type II pneumocyte hyperplasia
664 (thick arrow), bronchiolar epithelial hyperplasia, bronchiolar exudate (thin arrow) and edema
665 (asterisk). SARS-CoV-2 immunopositive cells are highlighted by brown triangles. Scale bars: Top
666 row, 1 mm; middle row, 50 µm; bottom row, 100 µm.

667

668 **Acknowledgments**

669 We thank Morgane Rolland for molecular phylogeny and Misook Choe for SpFN expression
670 consultation. We also thank Sebastian Molnar, Erin Kavusak, Jonah Heller, Claudelle Busano,

671 Hannah King, Sylriel Peters, Theron Jenifer and Jean-Paul Todd for technical support. We also
672 thank Mihret Amare, Mekdi Taddese, Jarrett Headley and Yahel Romem for programmatic
673 support and planning and Paul Scott scientific inputs and administrative oversight. This work was
674 funded by the US Department of Defense, Defense Health Agency was executed, in part, through
675 a cooperative agreement (W81XWH-18-2-0040) between the Henry M. Jackson Foundation for
676 the Advancement of Military Medicine, Inc., and the U.S. Department of Defense (DOD). Material
677 has been reviewed by the Walter Reed Army Institute of Research. The opinions or assertions
678 contained herein are the private views of the authors, and are not to be construed as official, or
679 as reflecting true views of the Department of the Army or the Department of Defense.

680

681 **Author contributions**

682 Conceptualization, D.L.B., M.G.J., N.L.M., K.M.; Investigation, K.MW., E.K.B, W-H.C., E.J.M., I.L-N.,
683 L.L.J., D.P-P., G.D.G, I.S., A.G., C.K., S.S., H.He., H.G., H.Ha., S.Ka., M.P., A.W., K.R., X.Z, M.R., S.A.P,
684 G.D.G, E.K.B., D.L.B., M.G.J., N.L.M., K.M.; Data Curation—K.MW., D.L.B., M.G.J. Essential
685 Reagents, R.S.S., A.A., E.B.M., P.M., S.J.K., A.S.P., J.R.C., M.S., G.R.M., E.A.B., D.C.D., R.A.S., Writing
686 – Original Draft, K.MW, D.L.B., N.L.M., K.M.; Writing – Review & Editing, All authors;
687 Visualization—K.MW., E.K.B., E.J.M., P.V.T, D.L.B., M.G.J., N.L.M. K.M.; Supervision—D.L.B.,
688 M.G.J., S.A.P., J.D., S.P.D., J.W.F., M.G.L., S.V., N.L.M., K.M.; Funding Acquisition—K.M., N.L.M.

689

690 **References**

691

- 692 1 Craven, J. (Regulatory Affairs Professionals Society, 2021).
- 693 2 Hu, B., Guo, H., Zhou, P. & Shi, Z. L. Characteristics of SARS-CoV-2 and COVID-19. *Nat Rev*
694 *Microbiol* **19**, 141-154, doi:10.1038/s41579-020-00459-7 (2021).

- 695 3 CDC. *SARS-CoV-2 Variant Classifications and Definitions*,
696 [https://www.cdc.gov/coronavirus/2019-ncov/cases-updates/variant-](https://www.cdc.gov/coronavirus/2019-ncov/cases-updates/variant-surveillance/variant-info.html#Concern)
697 [surveillance/variant-info.html#Concern](https://www.cdc.gov/coronavirus/2019-ncov/cases-updates/variant-surveillance/variant-info.html#Concern) (2021).
- 698 4 Wang, P. *et al.* Increased Resistance of SARS-CoV-2 Variants B.1.351 and B.1.1.7 to
699 Antibody Neutralization. *bioRxiv*, doi:10.1101/2021.01.25.428137 (2021).
- 700 5 Wibmer, C. K. *et al.* SARS-CoV-2 501Y.V2 escapes neutralization by South African COVID-
701 19 donor plasma. *Nat Med* **27**, 622-625, doi:10.1038/s41591-021-01285-x (2021).
- 702 6 Wu, K. *et al.* mRNA-1273 vaccine induces neutralizing antibodies against spike mutants
703 from global SARS-CoV-2 variants. *bioRxiv*, doi:10.1101/2021.01.25.427948 (2021).
- 704 7 Galloway, S. E. *et al.* Emergence of SARS-CoV-2 B.1.1.7 Lineage - United States, December
705 29, 2020-January 12, 2021. *MMWR Morb Mortal Wkly Rep* **70**, 95-99,
706 doi:10.15585/mmwr.mm7003e2 (2021).
- 707 8 Tegally, H. *et al.* Detection of a SARS-CoV-2 variant of concern in South Africa. *Nature* **592**,
708 438-443, doi:10.1038/s41586-021-03402-9 (2021).
- 709 9 Rambaut, A., Loman, N., Pybus, O., Barclay, W., Barrett, J., Carabelli, A., Connor, T.,
710 Peacock, T., Robertson, DL., Volz, E., on behalf of COVID-19 Genomics Consortium UK
711 (CoG-UK). *Preliminary genomic characterisation of an emergent SARS-CoV-2 lineage in the*
712 *UK defined by a novel set of spike mutations*, [https://virological.org/t/preliminary-](https://virological.org/t/preliminary-genomic-characterisation-of-an-emergent-sars-cov-2-lineage-in-the-uk-defined-by-a-novel-set-of-spike-mutations/563/1)
713 [genomic-characterisation-of-an-emergent-sars-cov-2-lineage-in-the-uk-defined-by-a-](https://virological.org/t/preliminary-genomic-characterisation-of-an-emergent-sars-cov-2-lineage-in-the-uk-defined-by-a-novel-set-of-spike-mutations/563/1)
714 [novel-set-of-spike-mutations/563/1](https://virological.org/t/preliminary-genomic-characterisation-of-an-emergent-sars-cov-2-lineage-in-the-uk-defined-by-a-novel-set-of-spike-mutations/563/1) (2020).
- 715 10 Hacısuleyman, E. *et al.* Vaccine Breakthrough Infections with SARS-CoV-2 Variants. *N Engl*
716 *J Med* **384**, 2212-2218, doi:10.1056/NEJMoa2105000 (2021).
- 717 11 Ho, D. *et al.* Increased Resistance of SARS-CoV-2 Variants B.1.351 and B.1.1.7 to Antibody
718 Neutralization. *Res Sq*, doi:10.21203/rs.3.rs-155394/v1 (2021).
- 719 12 Hu, J. *et al.* Emerging SARS-CoV-2 variants reduce neutralization sensitivity to
720 convalescent sera and monoclonal antibodies. *Cell Mol Immunol* **18**, 1061-1063,
721 doi:10.1038/s41423-021-00648-1 (2021).
- 722 13 Wang, P. *et al.* Antibody resistance of SARS-CoV-2 variants B.1.351 and B.1.1.7. *Nature*,
723 doi:10.1038/s41586-021-03398-2 (2021).
- 724 14 Wibmer, C. K. *et al.* SARS-CoV-2 501Y.V2 escapes neutralization by South African COVID-
725 19 donor plasma. *bioRxiv*, doi:10.1101/2021.01.18.427166 (2021).
- 726 15 Cohen, J. in *Science Magazine* (2021).
- 727 16 Garcia-Beltran, W. F. *et al.* Multiple SARS-CoV-2 variants escape neutralization by vaccine-
728 induced humoral immunity. *Cell*, doi:10.1016/j.cell.2021.03.013 (2021).
- 729 17 Alving, C. R., Peachman, K. K., Matyas, G. R., Rao, M. & Beck, Z. Army Liposome
730 Formulation (ALF) family of vaccine adjuvants. *Expert Rev Vaccines* **19**, 279-292,
731 doi:10.1080/14760584.2020.1745636 (2020).
- 732 18 Joyce, M. G. *et al.* Efficacy of a Broadly Neutralizing SARS-CoV-2 Ferritin Nanoparticle
733 Vaccine in Nonhuman Primates. *bioRxiv*, doi:10.1101/2021.03.24.436523 (2021).
- 734 19 King, H. A. D. *et al.* Efficacy and breadth of adjuvanted SARS-CoV-2 receptor-binding
735 domain nanoparticle vaccine in macaques. *bioRxiv*, doi:10.1101/2021.04.09.439166
736 (2021).
- 737 20 Joyce, M. G. *et al.* SARS-CoV-2 ferritin nanoparticle vaccines elicit broad SARS coronavirus
738 immunogenicity. *bioRxiv*, doi:10.1101/2021.05.09.443331 (2021).

- 739 21 Chan, J. F. *et al.* Simulation of the Clinical and Pathological Manifestations of Coronavirus
740 Disease 2019 (COVID-19) in a Golden Syrian Hamster Model: Implications for Disease
741 Pathogenesis and Transmissibility. *Clin Infect Dis* **71**, 2428-2446, doi:10.1093/cid/ciaa325
742 (2020).
- 743 22 Sia, S. F. *et al.* Pathogenesis and transmission of SARS-CoV-2 in golden hamsters. *Nature*
744 **583**, 834-838, doi:10.1038/s41586-020-2342-5 (2020).
- 745 23 Imai, M. *et al.* Syrian hamsters as a small animal model for SARS-CoV-2 infection and
746 countermeasure development. *Proc Natl Acad Sci U S A* **117**, 16587-16595,
747 doi:10.1073/pnas.2009799117 (2020).
- 748 24 Tostanoski, L. H. *et al.* Ad26 vaccine protects against SARS-CoV-2 severe clinical disease in
749 hamsters. *Nat Med* **26**, 1694-1700, doi:10.1038/s41591-020-1070-6 (2020).
- 750 25 Munoz-Fontela, C. *et al.* Animal models for COVID-19. *Nature* **586**, 509-515,
751 doi:10.1038/s41586-020-2787-6 (2020).
- 752 26 Hoffmann, M. *et al.* SARS-CoV-2 Cell Entry Depends on ACE2 and TMPRSS2 and Is Blocked
753 by a Clinically Proven Protease Inhibitor. *Cell* **181**, 271-280 e278,
754 doi:10.1016/j.cell.2020.02.052 (2020).
- 755 27 Fischer, R. J. *et al.* ChAdOx1 nCoV-19 (AZD1222) protects hamsters against SARS-CoV-2
756 B.1.351 and B.1.1.7 disease. *bioRxiv*, doi:10.1101/2021.03.11.435000 (2021).
- 757 28 CDC. *COVID Data Tracker* < [https://covid.cdc.gov/covid-data-](https://covid.cdc.gov/covid-data-tracker/?CDC_AA_refVal=https%3A%2F%2Fwww.cdc.gov%2Fcoronavirus%2F2019-ncov%2Fcases-updates%2Fvariant-proportions.html#variant-proportions)
758 [tracker/?CDC_AA_refVal=https%3A%2F%2Fwww.cdc.gov%2Fcoronavirus%2F2019-](https://covid.cdc.gov/covid-data-tracker/?CDC_AA_refVal=https%3A%2F%2Fwww.cdc.gov%2Fcoronavirus%2F2019-ncov%2Fcases-updates%2Fvariant-proportions.html#variant-proportions)
759 [ncov%2Fcases-updates%2Fvariant-proportions.html#variant-proportions](https://covid.cdc.gov/covid-data-tracker/?CDC_AA_refVal=https%3A%2F%2Fwww.cdc.gov%2Fcoronavirus%2F2019-ncov%2Fcases-updates%2Fvariant-proportions.html#variant-proportions) > (2021).
- 760 29 Karim, F. M., MYS; Gosnell, BI; Cele, S; Giandhari, J; Pillay, S; Tegally, H; Wilkinson, E; San,
761 JE; Msomi, N; Mlisana, K; Khan, K; Bernstein, M; Manickchand, N; Singh, L; Ramphal, U;
762 COMMIT-KZN Team, Hanekom, W; Lessells, RJ; Sigal, A; de Oliveira, T. Persistent SARS-
763 CoV-2 infection and intra-host evolution in association with advanced HIV infection.
764 doi:<https://doi.org/10.1101/2021.06.03.21258228> (2021).
- 765 30 Schafer, A. *et al.* Antibody potency, effector function, and combinations in protection and
766 therapy for SARS-CoV-2 infection in vivo. *J Exp Med* **218**, doi:10.1084/jem.20201993
767 (2021).
- 768 31 Suryadevara, N. *et al.* Neutralizing and protective human monoclonal antibodies
769 recognizing the N-terminal domain of the SARS-CoV-2 spike protein. *bioRxiv*,
770 doi:10.1101/2021.01.19.427324 (2021).
- 771 32 Suryadevara, N. *et al.* Neutralizing and protective human monoclonal antibodies
772 recognizing the N-terminal domain of the SARS-CoV-2 spike protein. *Cell* **184**, 2316-2331
773 e2315, doi:10.1016/j.cell.2021.03.029 (2021).
- 774 33 Winkler, E. S. *et al.* Human neutralizing antibodies against SARS-CoV-2 require intact Fc
775 effector functions for optimal therapeutic protection. *Cell* **184**, 1804-1820 e1816,
776 doi:10.1016/j.cell.2021.02.026 (2021).
- 777 34 Winkler, E. S. *et al.* Human neutralizing antibodies against SARS-CoV-2 require intact Fc
778 effector functions and monocytes for optimal therapeutic protection. *bioRxiv*,
779 doi:10.1101/2020.12.28.424554 (2020).
- 780 35 Mercado, N. B. *et al.* Publisher Correction: Single-shot Ad26 vaccine protects against
781 SARS-CoV-2 in rhesus macaques. *Nature* **590**, E25, doi:10.1038/s41586-020-03100-y
782 (2021).

- 783 36 Mercado, N. B. *et al.* Single-shot Ad26 vaccine protects against SARS-CoV-2 in rhesus
784 macaques. *Nature* **586**, 583-588, doi:10.1038/s41586-020-2607-z (2020).
- 785 37 Yu, J. *et al.* DNA vaccine protection against SARS-CoV-2 in rhesus macaques. *Science* **369**,
786 806-811, doi:10.1126/science.abc6284 (2020).
- 787 38 Corbett, K. S. *et al.* Evaluation of the mRNA-1273 Vaccine against SARS-CoV-2 in
788 Nonhuman Primates. *N Engl J Med* **383**, 1544-1555, doi:10.1056/NEJMoa2024671 (2020).
- 789 39 Hoffmann, D. C., B; Rauch, S; Roth, N; Mühe, J; Halwe, NJ; Ulrich, L; Fricke, C; Schön, J;
790 Kraft, A; Breithaupt, A; Wernike, K; Michelitsch, A; Sick, F; Wylezich, C; Müller, SO;
791 Mettenleiter, TC; Petsch, B; Dorhoi, A; Beer, M. CVnCoV protects human ACE2 transgenic
792 mice from ancestral B BavPat1 and emerging B.1.351 SARS-CoV-2. *bioRxiv*,
793 doi:<https://doi.org/10.1101/2021.03.22.435960> (2021).
- 794 40 Carmen, J. S., S; Lu, Z; Anderson, A; Morrison, EB; Sankhala, RS; Chen, W-H; Chang, WC;
795 Bolton, JS; Matyas, GR; Michael, NL; Joyce, MG; Modjarrad, K; Currier, JR; Bergmann-
796 Leitner, E; Malloy, AMW; Rao, M. A spike-ferritin nanoparticle vaccine induces robust
797 innate immune activity and drives polyfunctional SARS-CoV-2-specific T cells.
798 doi:<https://doi.org/10.1101/2021.04.28.441763> (2021).
- 799 41 Tegally, H. e. a. Emergence and rapid spread of a new severe acute respiratory syndrome-
800 related coronavirus 2 (SARS-CoV-2) lineage with multiple spike mutations in South Africa.
801 *medRxiv*, doi:<https://doi.org/10.1101/2020.12.21.20248640> (2020).
802
803

804 **Supplemental material**

805

806 **Supplemental Figure 1. Additional antibody responses following SpFN-ALFQ immunization. a,**

807 ELISA was performed using either WA1 derived Receptor Binding Domain (RBD) or S-2P Spike

808 proteins from sera taken at week 8. The vaccine regimens are indicated on the x-axis by

809 phosphate buffered saline (PBS) control or SpFN dose with the number of vaccinations in the

810 regimen given parenthetically and by color code (blue, 2-dose, red, 1-dose). Endpoint titers are

811 given on the y-axis as geometric mean titers with data displayed in box plots with the top and

812 bottom bars of the box the standard deviation and the middle bar as the median value. P-values

813 for SpFN-ALFQ vaccination groups compared with PBS control are given just above the boxes in

814 light grey while inter- and intra-regimen p-values are given above the boxes in black. ns, not

815 significant ($p > 0.05$). **b,** Octet Biolayer Interferometry (BLI) responses against the WA1, B.1.1.7,

816 and B.1.351 sequences of the RBD are given for the vaccination regimens as in **a** on the x-axis

817 from sera collected at week 8. BLI responses are given in nanometers (nm) on the y-axis.

818 Vaccination regimen color coding and statistical treatments are as in **a**. **c,** IgG opsonization as

819 measured by binding to SARS-CoV-2 Spike protein expressing expi293F cells subsequently stained

820 by fluorescently tagged goat anti-hamster IgG and detected by flow cytometry. Fluorescence is

821 given as mean fluorescence intensity (MFI) on the y-axis. Vaccination regiment color coding and

822 statistical treatments are as in **a**.

823

824 **Supplemental Fig 2. Quantitative SARS-CoV-2 total and subgenomic mRNA (sgmRNA) viral load**

825 **from oral swabs following challenge.** Oral fluid collection from were obtained by swabbing at

826 days 2, 4, and 6 post challenge in hamsters and submitted to quantitative SARS-CoV-2 total and

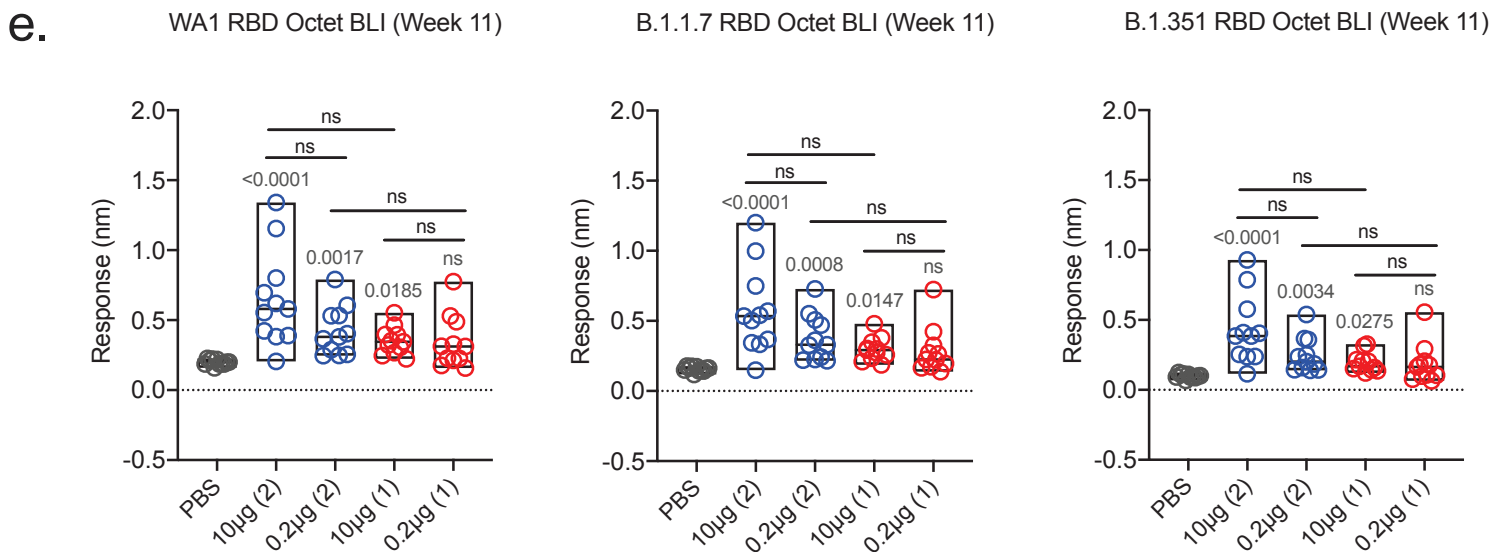
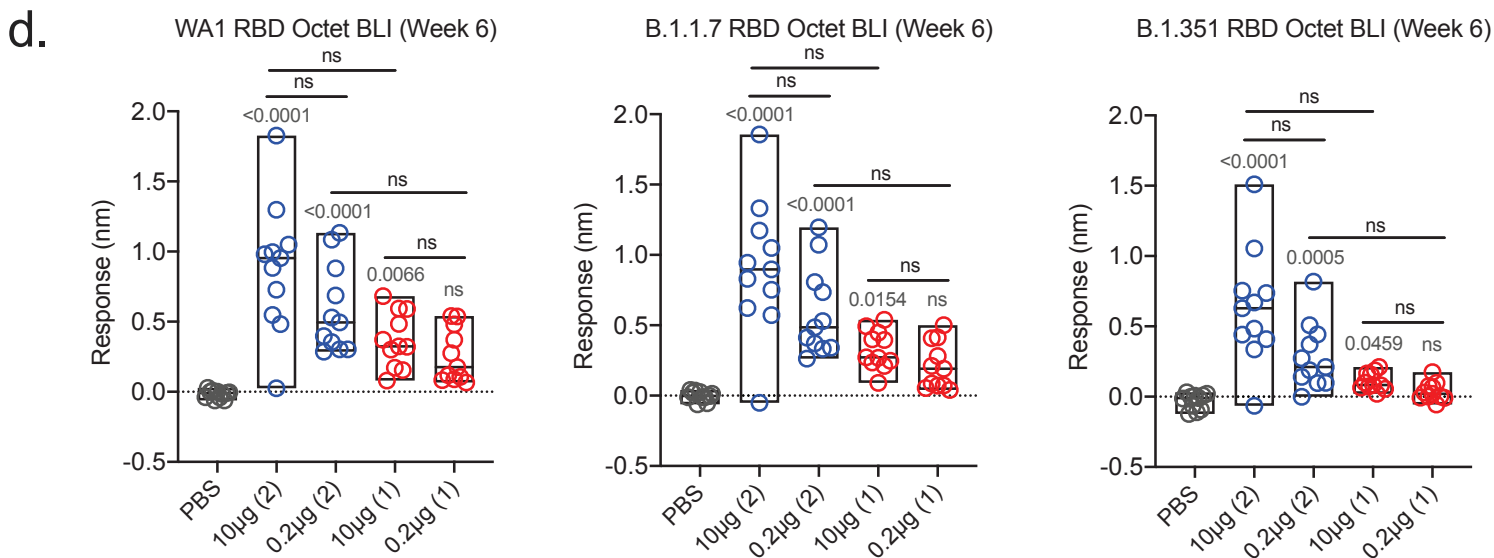
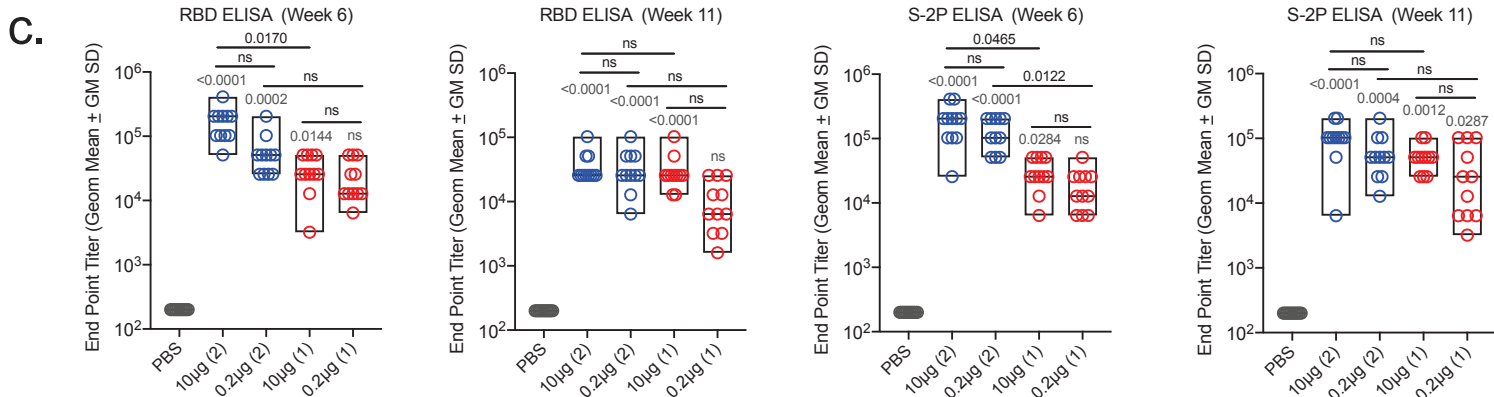
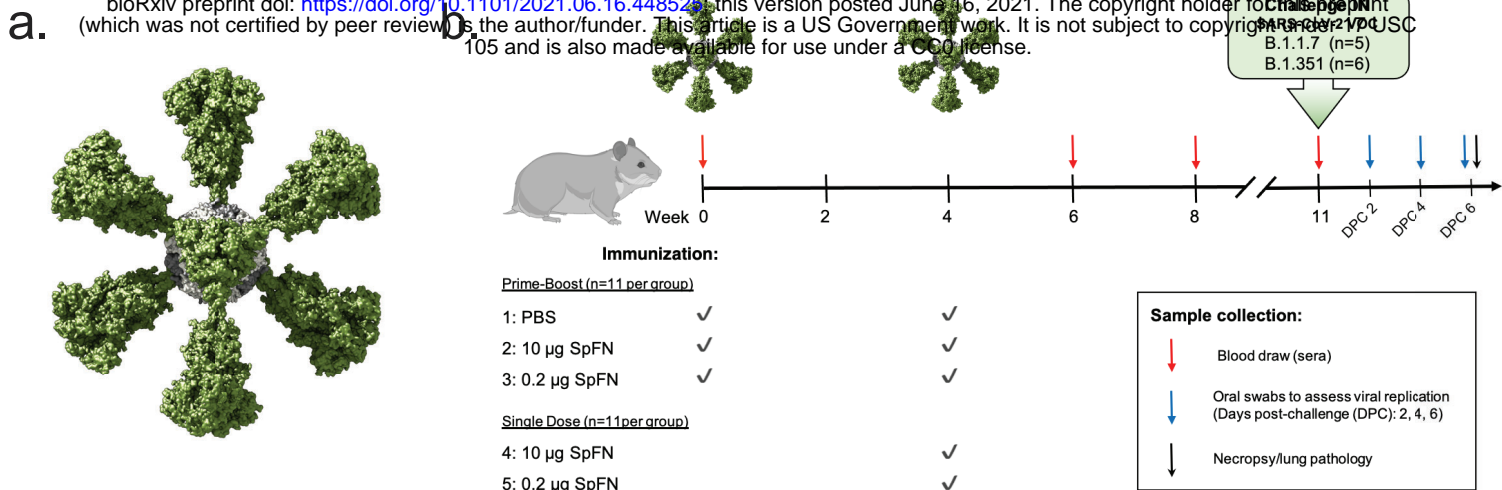
827 sgmRNA analysis. Viral load is given on y-axes at copies/mL of oral fluid plotted on a log₁₀ scale.
828 Vaccination regimen groups, stratified by day post-challenge, are given on the x-axes: Phosphate
829 buffered saline (PBS) control, gray circles; 10 µg and 0.2 µg 2-dose regimen groups, blue circles;
830 10 µg and 0.2 µg 1-dose regimen groups, red circles. Data are given in box plots where the
831 horizontal bar is the median value for each group. Where values between groups are statistically
832 meaningfully different, p-values are given above horizontal black bars showing the analyzed
833 groups. In all other cases, the p-values were > 0.05. **a**, sgmRNA viral load from B.1.1.7 challenged
834 hamsters; **(B)** total RNA viral load from B.1.1.7 challenged hamsters; **c**, sgmRNA viral load from
835 B.1.351 challenged hamsters; **d**, total RNA viral load from B.1. 351 challenged hamsters.

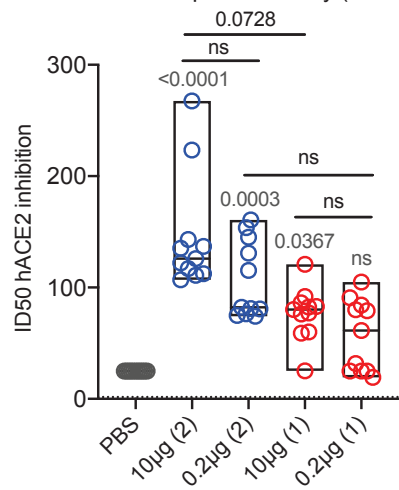
836

837 **Supplemental Table 1. Semi-quantitative histopathology and IHC scores**

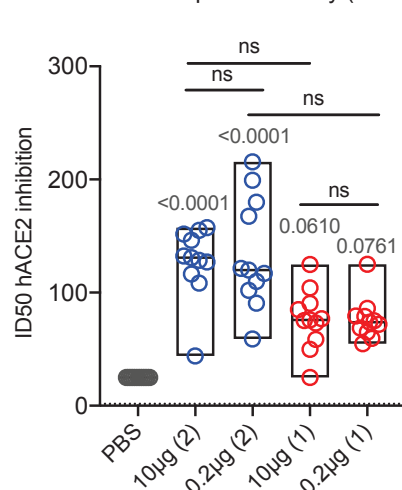
838 Lung tissues were collected at necropsy on day 6 post-challenge, fixed with neutral buffered
839 formalin, and stained with hematoxylin and eosin (H&E) for standard microscopic examination
840 as well as submitted for immunohistochemical (IHC) staining for SARS-CoV-2 nucleocapsid (N)
841 protein. (A) H&E sections were semi-quantitatively scored on the histopathology present in all
842 lung sections examined (Methods). The overall severity of interstitial pneumonia (IP) present in
843 individual animals in the PBS control and vaccinated groups is given. (B) IHC sections were
844 examined at 400X magnification, and evaluated for the number of immunopositive cells per slide.
845 Distribution of the number of immunopositive cells per section is given per PBS control and 2-
846 dose and 1-dose vaccine group. The number of vaccinations per vaccine group are given
847 parenthetically.

848

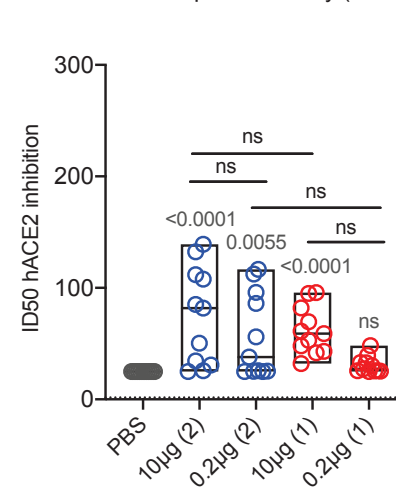
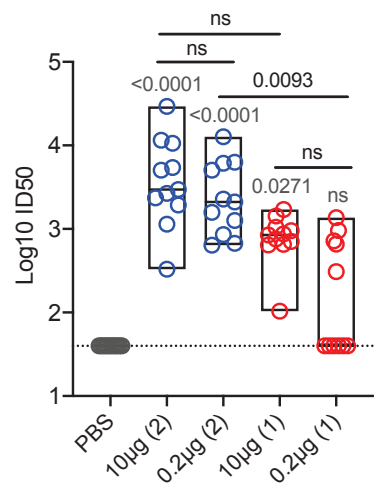


a. hACE2 Competition Assay (Week 6)

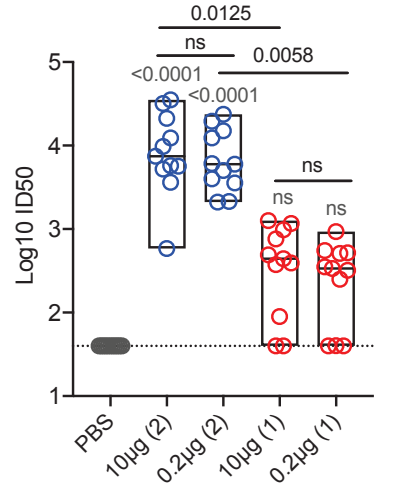
hACE2 Competition Assay (Week 8)



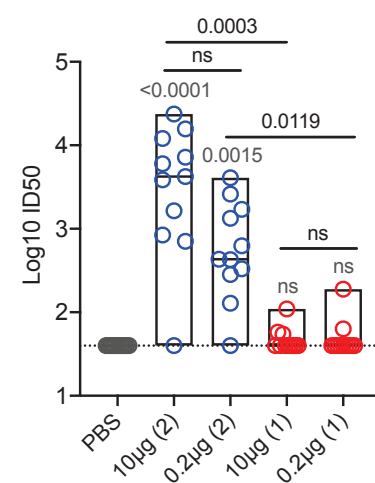
hACE2 Competition Assay (Week 11)

**b.** WA1 PSV Neutralization (Week 6)

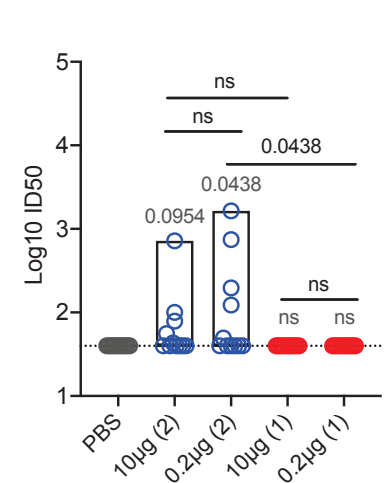
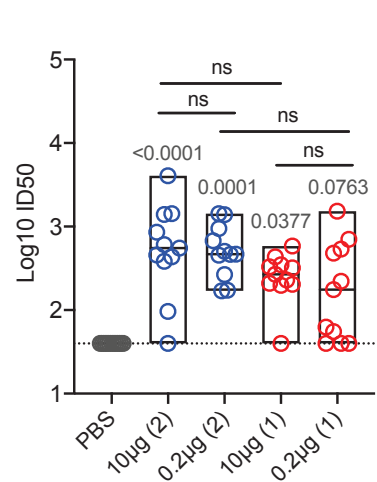
B.1.1.7 PSV Neutralization (Week 6)



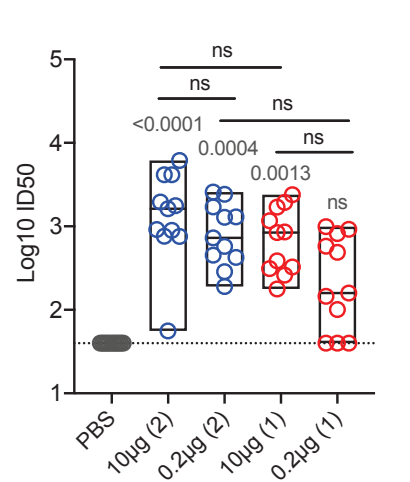
B.1.351 PSV Neutralization (Week 6)



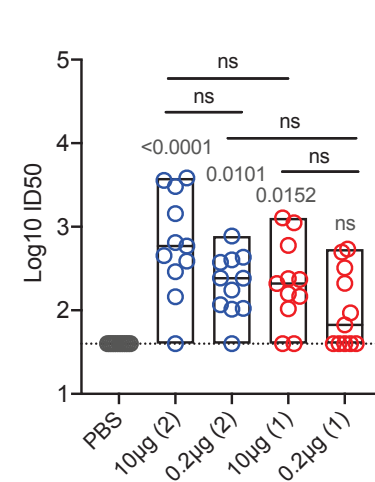
SARS1 PSV Neutralization (Week 6)

**c.** WA1 PSV Neutralization (Week 11)

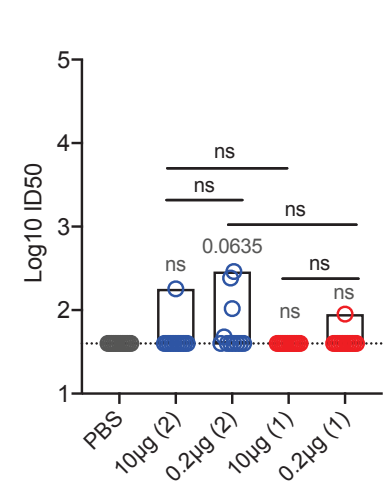
B.1.1.7 PSV Neutralization (Week 11)



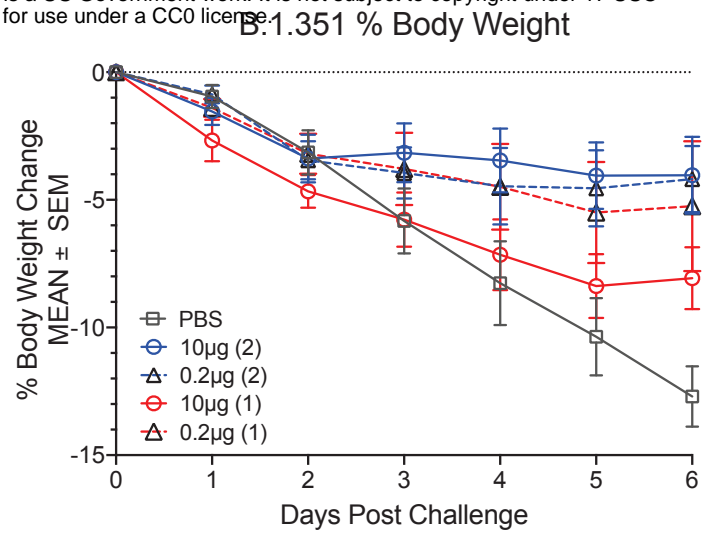
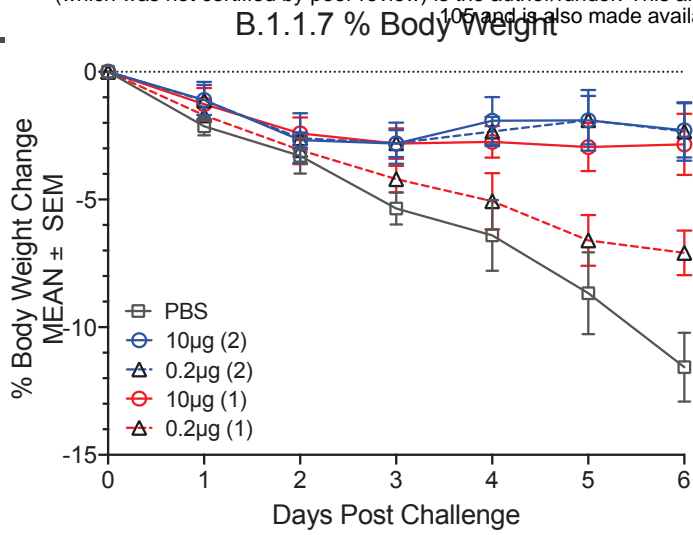
B.1.351 PSV Neutralization (Week 11)



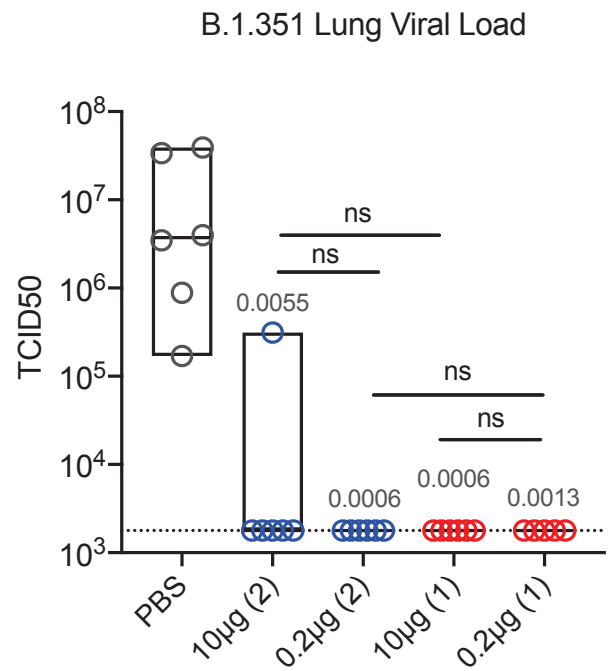
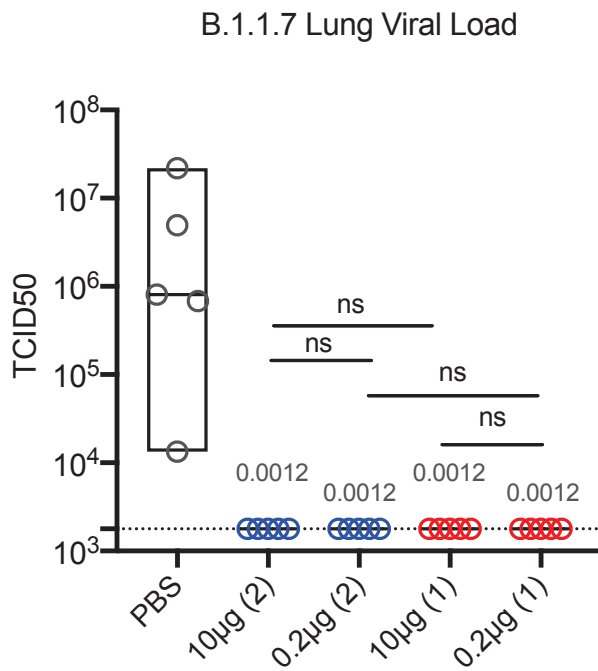
SARS1 PSV Neutralization (Week 11)



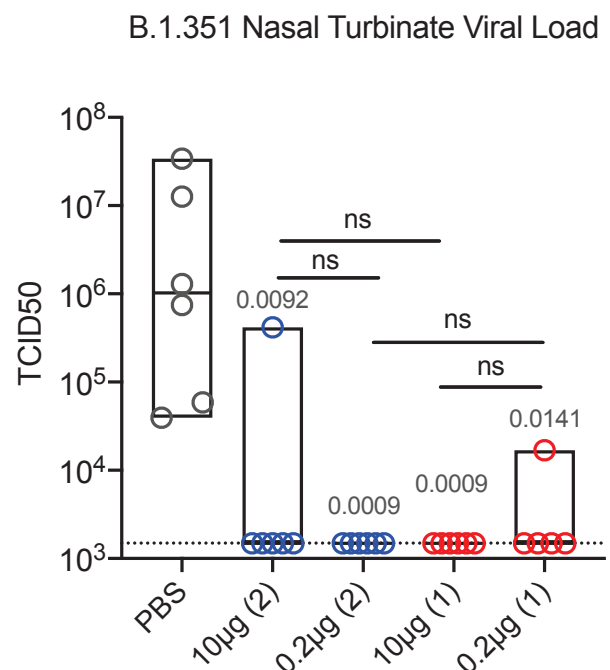
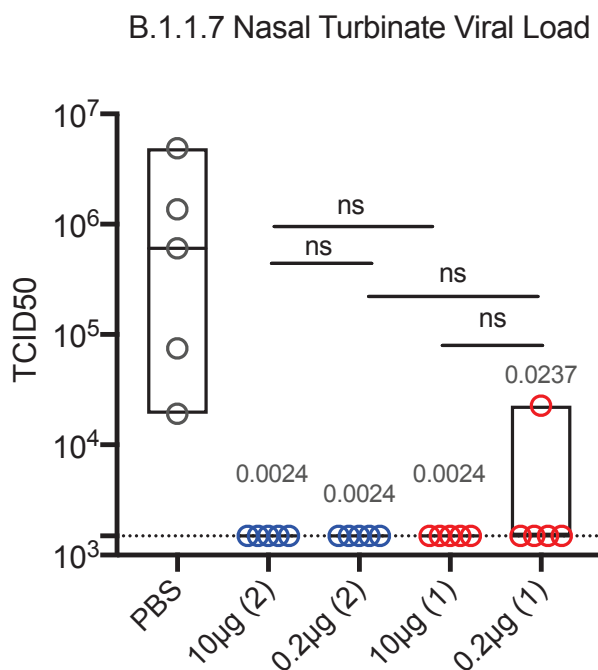
a.



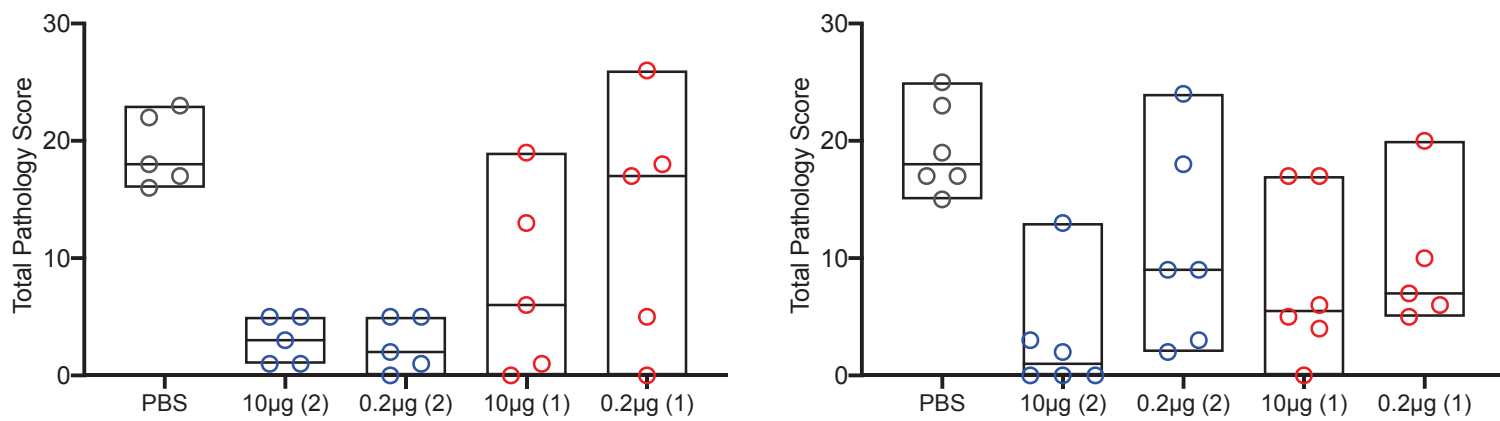
b.



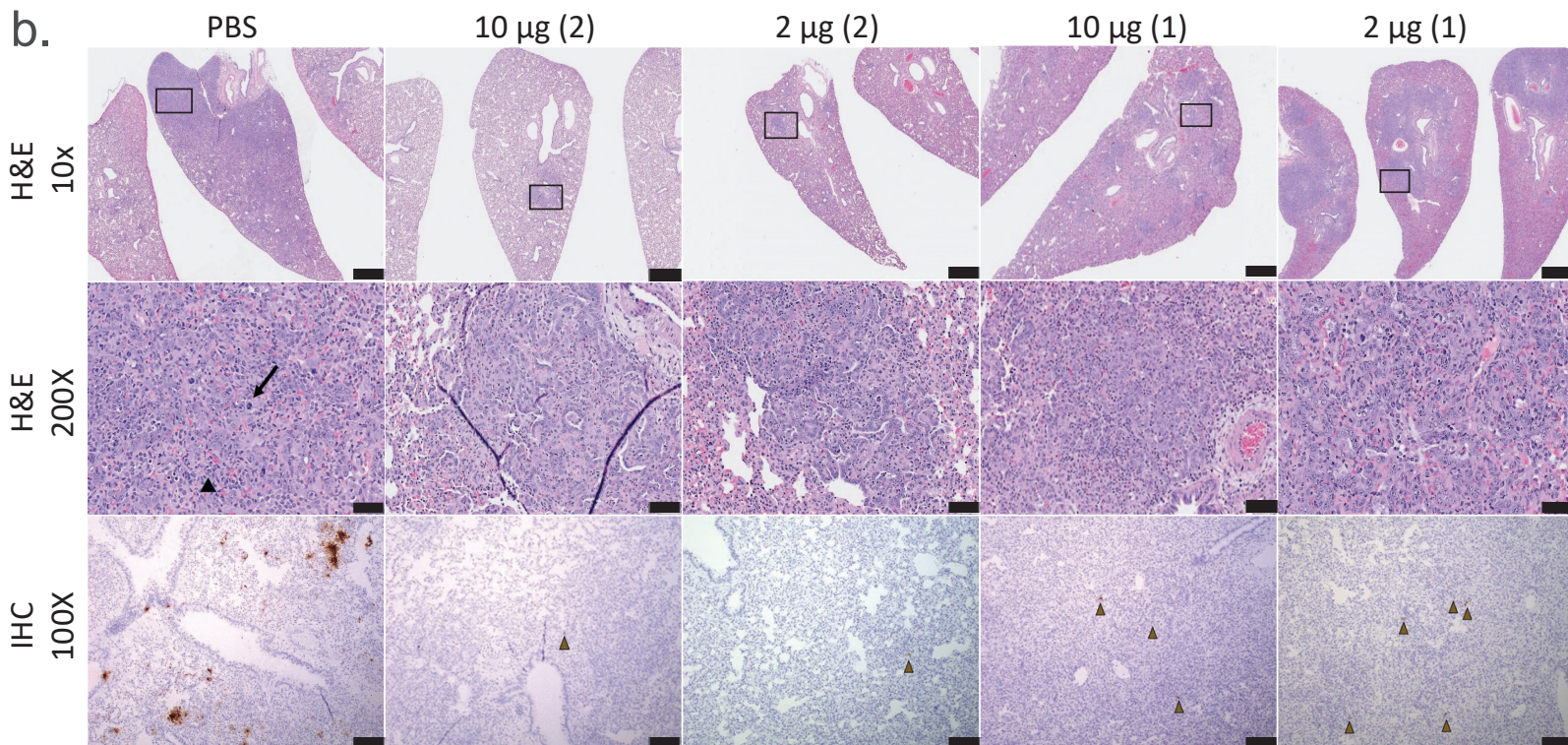
c.



a.



b.



c.

